Spatial distributed phosphatome determines EGFR phosphorylation response

Dissertation

Zur Erlangung des akademischen Grades eines

Doktors der Naturwissenschaften

(Dr. rer. nat.)

der Fakultät Chemie und Chemische Biologie

der Technischen Universität Dortmund

vorgelegt von

Amit Mhamane

December 2017

Vorgelegt im December 2017

von Amit Mhamane

Gutachter:

Prof. Dr. Philippe Bastiaens

Prof. Dr. Andrea Musacchio

The work presented in this dissertation was performed in the laboratory of

Prof. Dr. Philippe Bastiaens at the Max Planck Institute of Molecular Physiology,

Dortmund, Germany.

TABLE OF CONTENTS

ABBREVIATIONS

°C	Degree Celsius
a.u.	Arbitrary units
C-terminus	carboxy terminus
CA	Cell array
Cbl	Casitas B-lineage lymphoma proto-oncogene
cDNA	complementary DNA
DMEM	Dulbecco´s modified Eagle´s medium
DNA	deoxyribnucleic acid
dNTPs	deoxyribonucleoside triphosphates
EDTA	ethylenediamininetetraacetic acid
EGF	Epidermal growth factor
EGFR	Epidermal growth factor receptor
ER	endoplasmatic reticulum
FERM	4.1 protein ezrin radixin moesin
FLIM	Fluorecence liftime imaging microscopy
FRET	Förster resonance energy transfer
GFP	green fluorecent protien
HEPES	N-2-hydroxyethylpiperanzine-N´-2-ethanesulfonic-acid
Hz	hertz
MCF7	Michigan cancer foundation 7

min	minutes
mTFP	monomeric teal fluorescent protein
NADP	Nicotinamide adenine dinucleotide phosphate
NLS	nuclear localization sequence
NM	Nuclear membrane
NOX	NADPH oxidase
NRPTP	non-receptor PTP
ns	nanosecond
PM	plasma membrane
PTB	phosphotyrosine binding
PTP	protein tyrosine phosphatase
pY	phosphotyrosine
RNA	Ribonucleic acid
ROS	reactive oxygen species
RPTP	receptor-like protein tyrosine phosphatase
RT	room temperature
RTK	receptor tyrosine kinase
SH2	src homology 2
siRNA	small interfering RNA
Src	Proto-oncogene tyrosine-protein kinase Src
TM	transmembrane
WT	wild type
µl	microliter

ABSTRACT

Autocatalytic activation of Epidermal Growth Factor Receptor (EGFR) at the plasma membrane increases the sensitivity of the cell to extracellular growth factors but can also generate spontaneous receptor activation in the absence of stimulation. As a mechanism to control EGFR phosphorylation at the plasma membrane, receptor endocytosis and vesicular trafficking relocalizes activated, phosphorylated EGFR to perinuclear compartments rich in Protein Tyrosine Phosphatases (PTPs), such as PTPN1, which dephosphorylate and inactivate the receptor. Although the role of few PTPs in regulating EGFR phosphorylation is known, it is unclear how PTPs that are spatially segregated in distinct cellular compartments, modulate EGFR autocatalytic activation and hence its downstream signaling. Through quantitative imaging of EGFR phosphorylation upon genetic perturbations of classical PTPs and EGFR-PTP interactions, we identified endoplasmic reticulum (ER) associated PTPN2 and plasma membrane associated receptor-like PTPRG/J as strong, direct negative regulators of EGFR. Using single cell measurements of phosphorylation of the EGFR downstream signaling tyrosine residue Y1068, we generated a spatial-temporal reactivity map to identify local phosphatase activity. By negatively regulating EGFR phosphorylation, we deduced the role of PTPN2/PTPRJ in determining signal duration: a function that is coupled to vesicular trafficking. Furthermore, by maintaining the plasma membrane density of EGFR due to its interaction with ligandless EGFR and dephosphorylation of EGFR at Y1045 - a cCbl-ubiquitin ligase binding site, PTPN2 participates in a spatially established negative-feedback that is mediated by vesicular recycling. Through its activity on ligandless EGFR at plasma membrane, PTPRG regulates the autocatalytic activity of EGFR and influences the responsiveness of a cell to EGF dose. Altogether our findings indicate that by spatially segregating PTPs with different functional relationships to EGFR, the cell is able to sense and respond to its environment.

ZUSAMMENFASSUNG

Autokatalytische Aktivierung des epidermalen Wachstumsfaktor-Rezeptors (EGFR) an der Plasmamembran erhöht die Sensitivität der Zelle gegen gegenüber extrazellulären Wachstumsfaktoren, kann jedoch gleichzeitig auch spontane Aktivierung des Rezeptors in Abwesenheit eines Liganden erzeugen. Ein Mechanismus die Phosphorylierung von aktivierten EGFR an der Plasmamembran zu kontrollieren beinhaltet Rezeptor-Endozytose und vesikulärer Transport des Rezeptors durch perinukleäre Kompartimente welche eine hohe Konzentration an Protein Tyrosin Phosphatasen (z.B. PTPN1) aufweisen und den Rezeptor durch Dephosphorylierung inaktivieren. Bisher ist nur von wenigen PTPs die Rolle bei der Regulation der EGFR-Phosphorylierung bekannt, weiterhin ist es unklar, wie PTPs, die in verschiedenen zellulären Kompartimenten räumlich getrennt sind, die autokatalytische EGFR-Aktivierung und Signalweiterleitung modulieren. Durch quantitative Mikroskopie der Phosphorylierung von EGFR in Kombination mit genetischen Störungen klassischer PTPs und EGFR-PTP-Interaktionen wurden die mit dem endoplasmatischen Retikulum (ER) assoziierte Phosphatase PTPN2 und die Plasmamembran-assoziierten, Rezeptor-ähnlichen Phosphatasen PTPRG/J als starke, direkte Regulatoren von EGFR identifiziert. Mittels Einzelzellmessungen der Phosphorylierung des EGFR-Downstream-Signaltyrosinrests Y1068 wurden räumlich-zeitliche Reaktivitätskarten um die lokale Phosphatase-Aktivität zu bestimmen. Hierbei wurde eine an vesikuläreren Transport gekoppelte negative regulatorische Funktion von PTPN2/PTPRJ abgeleitet, welche die Dauer der Signalweiterleitung bestimmt. Weiterhin wurde gezeigt, das PTPN2 durch Interaktion mit ligandenfreiem EGFR und Dephosphorylierung der Bindestelle (Y1045) der Ubiquitin-Ligase cCbl die Dichte von EGFR an der Plasmamembran mittels vesikuläreren Transport reguliert. Durch Interaktion mit ligandenfreiem EGFR an der Plasmamembran reguliert PTPRG die autokatalytische Aktivität von EGFR und beeinflusst so die Reaktivität der Zelle gegenüber verschiedenen EGF Konzentrationen. Zusammenfassend zeigen diese Ergebnisse, dass durch räumliche Trennung von PTPs mit unterschiedlichen funktionellen Beziehungen zu EGFR die Zelle in der Lage ist, ihre Umgebung zu erkennen und darauf zu reagieren.

INTRODUCTION

1.1 CELL SIGNALING

A cell senses extracellular cues through its respective receptors present on its plasma membrane. Depending upon the strength of this stimuli, which is a reflection of the concentration of the chemical cue, the receptors are activated, in most cases leading to a conformational change that elevates their enzymatic activity(Lemmon and Schlessinger, 2010; Reynolds et al., 2003). The most common receptors are protein based tyrosine kinases that phosphorylate the tyrosine residues of their substrate (Figure 1-1)(Arkhipov et al., 2013; Kovacs et al., 2015). The activated receptor allows the cell to transmit an active signal through modification of various other spatially distributed downstream signaling proteins. The flow of such a signaling cascade is terminated when the activated protein is degraded or

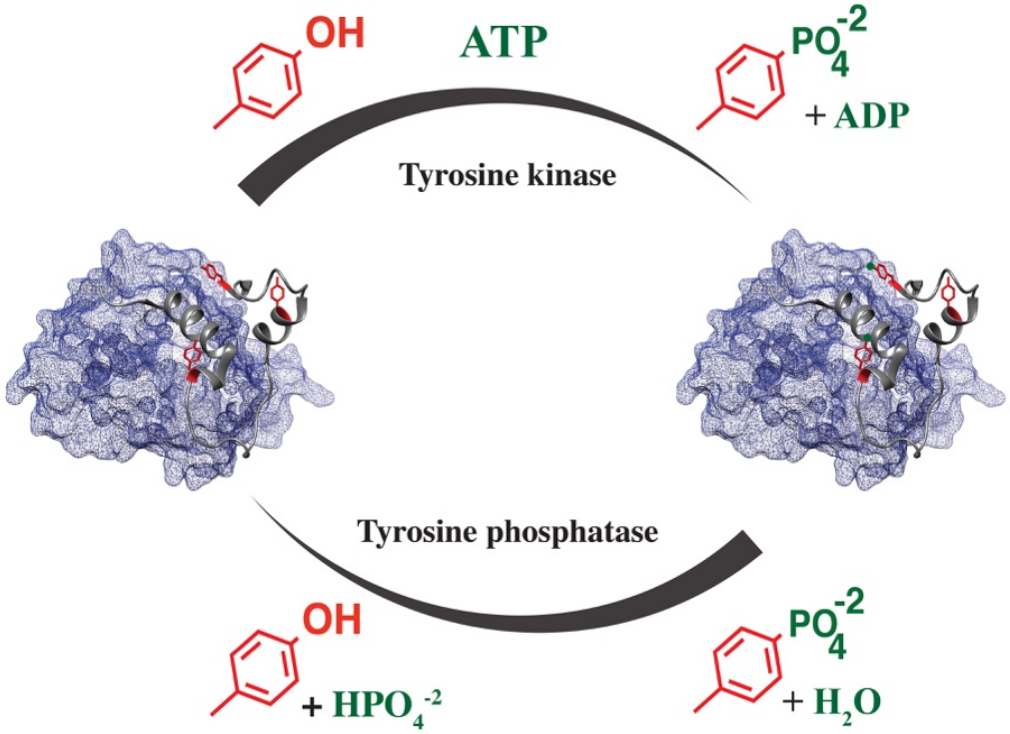

Figure 1-1 Schematic representing protein tyrosine phosphorylation-dephosphorylation cycle. PDB ID: 4G5J

is deactivated by a class of proteins called phosphatases (Haj, 2002; Tao et al., 2001). The conventional thought of perceiving signaling tracks as a linear pathway has been challenged due to the presence of recurring regulatory or feedback circuits between different signaling components. The spatial-temporal dynamics of signaling network, therefore, helps maintaining homeostasis or facilitates adaptation to a new environment.

Until the first discovery of the tyrosine kinase v-Src by Prof Ray Erikson, which was later characterized by Prof Tony Hunter for its role in tyrosine residues phosphorylation in proteins, the importance of the phosphorylation-dephosphorylation cycle was limited to the metabolism (Gschwind et al., 2004; Hunter and Cooper, 1985; Robinson et al., 2000; Ségaliny et al., 2015). Protein-tyrosine kinases (PTKs) are known to phosphorylate tyrosine residues of their protein substrate by transferring gamma phosphate of ATP (Figure 1-1). It was the discovery of various other tyrosine kinases like INSR, JAKs, STAT and MAPKs, in the 1990s that started to fill the gaps in the knowledge of the protein kinase cascades and their role in regulating cellular function. Sequencing of the human genome lead to the identification of 90 active TK genes; out of which 58 encode receptor TKs and 32 genes for non-receptor TKs(Robinson et al., 2000). Tyrosine kinases participate and monitor various cellular functions and the fact that they form a major fraction of all the known oncogenes makes understanding their role even more important (Regad, 2015; Robinson et al., 2000).

1.2 Epidermal growth factor receptor (EGFR)

EGFR is a member of ERBB family of RTKs and was among the first RTKs to be discovered. The EGF mediated activation of this protein intrigued the biochemists about its possible substrates and their role in cells (Ferguson, 2008). It was observed that this protein primarily acts as a substrate to its own enzymatic activity(Lemmon and Schlessinger, 2010). The fact that EGFR gets internalized upon EGF stimulation highlighted the possible role of

energy invested vesicular trafficking in signaling contrary to a simple diffusion-based model. Unravelling of the structure and the mechanisms of activation, identification of signaling adaptor proteins containing Src Homlogy 2 (SH2) and phosphor-tyrosine binding (PTB) domains, identification of the vesicular trafficking entities and discovery of first tyrosine phosphatase PTP1B translated our understanding of EGFR activity(Tonks, 2005).

1.2.1 The structure of EGFR shows regulation at different sites

Due to the difficulty in getting a crystal of an intact EGFR full length protein, the knowledge we have today about its structure are from NMR and X-ray data obtained from either external regions or internal parts. The EGFR monomer consists of an extracellular region, transmembrane domain, juxtamembrane region, a kinase domain and a C-terminal tail with regulatory tyrosine sites (Figure 1-2A).

External Domain: The external region comprises of four domains. The EGF binding pocket is formed by Domain I and Domain III and two cysteine rich domains Domain II and Domain IV(Klein et al., 2004). In the absence of ligand, the interaction of Domain II with Domain IV leads to a closed conformation of the EGFR monomer(Ferguson, 2008; Ogiso et al., 2002). Upon ligand binding to Domain I and Domain III, there is a structural rearrangement that exposes the dimerization arm in Domain II that can interact with other receptors to form a dimer. Domain IV plays a role in altering the binding affinity towards EGF or in mediating the higher oligomerization states of EGFR. As a dimer, one EGFR molecule interacts with other EGFR molecule in a back-to-back conformation through the dimerization arm making this a receptor mediated interaction rather than ligand mediated (Gan et al., 2007)(Figure 1-2B).

TRANSMEMEBRANE-JUXTAMEMBRANE REGION: The juxta-membrane region of EGFR has an auto-inhibitory role that entraps the monomeric EGFR in an inactive state(Shan et al., 2012). The conformational change induced due to ligand binding releases this auto-inhibition, affecting the orientation of JM-TM in the formation of dimeric EGFR, now, in an active state. Although the monomeric form of EGFR was always considered to be an inactive state, this does not imply that the kinase activity of EGFR is shut down. Recent studies have shown that even in a monomeric state, EGFR has a weak kinase activity that facilitates lower amplitude downstream signaling in the absence of a ligand(Baumdick et al., 2015). It has also been reported that the phosphorylation of the threonine residues of EGFR

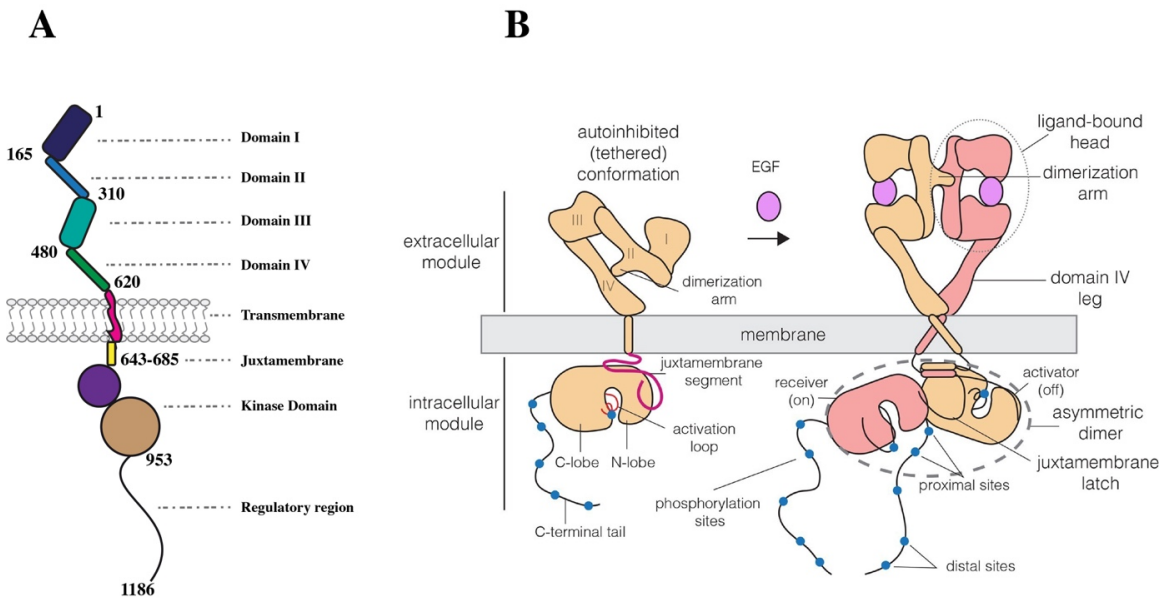

Figure 1-2 A) Schematic representation of the EGFR structure. A single transmembrane domain connects the extracellular ligand-binding domain with the cytosolic part of EGFR. The cytosolic domain is further separated to the juxtamembrane segment, the tyrosine kinase domain with the αC-helix and activation loop, and the C-terminal tail with several tyrosine residues. Mechanism of EGFR activation. **B)** Ligand binding to EGFR results in the formation of an asymmetric dimer, where one receptor acts as an 'activator' and the second one as a 'receiver'. Tyrosine phosphorylation at the C tail of the 'receiver' kinase can only occur if the receptors dynamically change their positions (Adapted from Jura et al., 2009).

(T654/T669) in the juxta-membrane by ERK affects the oligomerization step and maintains EGF-EGFR molecules in the monomeric state(Kluba et al., 2015).

KINASE DOMAIN: The EGFR kinase domain comprises of two lobes: C-lobe and N lobe. The C-lobe (activator) of one EGFR molecule interacts with the N-lobe (the receiver) of the kinase domain of the binding partner kinase. This interaction leads to the formation of an asymmetric dimer. This stabilizes the EGF mediated allosterically activated conformation of the receiver kinase domain. The kinase domain also contains the lysine residues that act as a substrate to ubiquitin ligases like cCBL which controls affects ubiquitination and thus tags EGFR for endosomal sorting. The structural and molecular dynamics simulations suggested that Y845 phosphorylation in the activation loop suppresses the intrinsic disorder in the ✔C-helix, thereby stabilizing the active conformation (Shan et al., 2012). If this active conformation would further catalyze Y845 phosphorylation on other EGFR molecules thereby further stabilizing EGFR molecules in an active conformation this would provide the basis for autocatalytic amplification of EGFR activity (Reynolds et al., 2003; Tischer and Bastiaens, 2003).

EGFR C-TERMINAL TAIL: At the C terminal end, EGFR consists of a 229aa peptide that harbors autophosphorylation tyrosine sites with signaling and trafficking potential. Phosphorylation of Y845 avails autocatalytic function to EGFR that plays an important role in the lateral signal propagation. The mechanism by which pY845 is able to carry out this function has not been shown experimentally but simulation data indicates that it might be due to its capability to suppresses the intrinsic disorder of EGFR. Ligand induced autophosphorylation of Y992, Y1068, Y1086, Y1148, and Y1173 acts as a docking sites for adapter proteins like Grb2 and Shc to trigger downstream signaling. In addition to EGFR bound Grb2, E3 ubiquitin ligase c-Cbl also binds to pY1045 of EGFR.

1.2.2 EGFR DOWNSTREAM SIGNALING

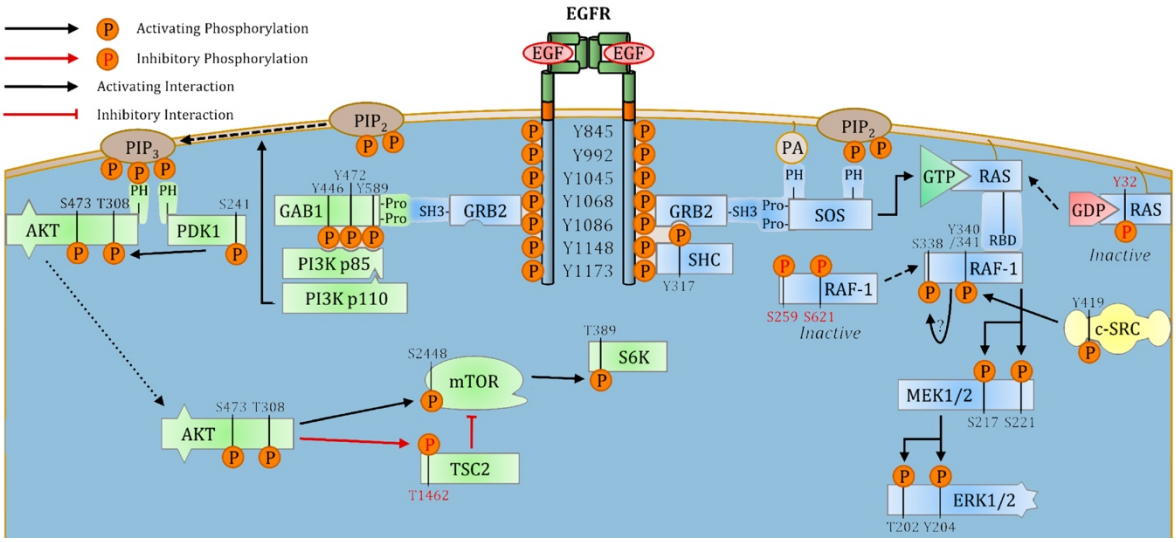

Figure 1-3 Schematic showing an overview about the major downstream signaling initiated by auto phosphorylation of EGFR tyrosine sites shown in orange. The figure has been adapted from (Morandell et al., 2008).

Activation of EGFR might lead to different cellular fates like survival, proliferation or apoptosis. Proteins with SH2 or PTB domain typically recognize a pTyr residue orchestrated by a specific amino acid sequence(Wagner et al., 2013). Their recruitment to these sites stimulate recruitment of other proteins and assembling of complexes that result in activation of the downstream signaling proteins. Upon phosphorylation of pY1068 /pY1086 of EGFR, Grb2 binds to these sites due to its SH2 domains(Sorkin et al., 2000). Through its SH3 domains, GRB2 is bound to SOS (Son of Sevenless), which is thus recruited to the plasma membrane. The increased proximity of SOS to membrane bound RAS results in increased nucleotide exchange on Ras (Wee and Wang, 2017). The GTP bound RAS now phosphorylate Raf kinase that in turn activates ERK in a MEK dependent manner(Fey et al., 2016). An active cytoplasmic ERK shuttles to the nucleus and increase the transcription of cFOS. The other major downstream protein that is activates through EGFR is AKT(Gan et

al., 2010). Involvement of EGFR pY1173 bound Shc protein in activating AKT is arguable, the commonly accepted mechanism is via a Grb2-Gab1 complex(Keilhack et al., 1998). PI3K is recruited and activated on the cell membrane by interacting with phosphorylated Gab. PI3K converts PIP2 to PIP3 which then acts as a binding partner for both AKT and its activator PDK(Wee and Wang, 2017). PDK phosphorylates T308 of the AKT while the S473 is phosphorylated by mTOR(Nishimura et al., 2015). The role of Grb2 in mediating both AKT and ERK signals indicates that the signaling does not follow a fixed pathway. The activation state of EGFR, magnitude of its phosphorylation, spatial distribution and availability of the accessory proteins collectively determines the signaling outcome.

A sustained ERK response leads to activation of cFOS and further increases its expression. cFOS is a transcription factor that increases expression of other proliferation associated gene(Wu et al., 2012)s. A transient ERK response, however, activates less amount of cFOS which is degraded immediately. This demonstrates that the cellular decision depends on the temporal response profile of an RTK and their downstream signaling proteins, and thus regulation of these profiles becomes an important mechanism. EGFR is known to be regulated by two mechanisms; Either it is degraded in the lysosome which affects the total concentration in the cell or it is dephosphorylated by protein tyrosine phosphatases which affects the activity. Both of these mechanisms are highly dependent on the vesicular trafficking system of a cell.

1.3 EGFR Regulation by vesicular trafficking

The two common mechanism of EGFR internalization is mediated by Clathrin coated vesicles or Caveolae rafts mediated vesicles(Mayor et al., 2017) (Figure 1-4). Although, both of these mechanisms are dependent on receptor ubiquitination their role in receptor sorting and signaling is still unclear. The receptor vesicles are then converged to the early endosome.

The early endosome acts as a distributing hub wherein Rab5-positive vesicles mature into Rab7-late endosomes, which are then fused to the lysosome that contains proteolytic

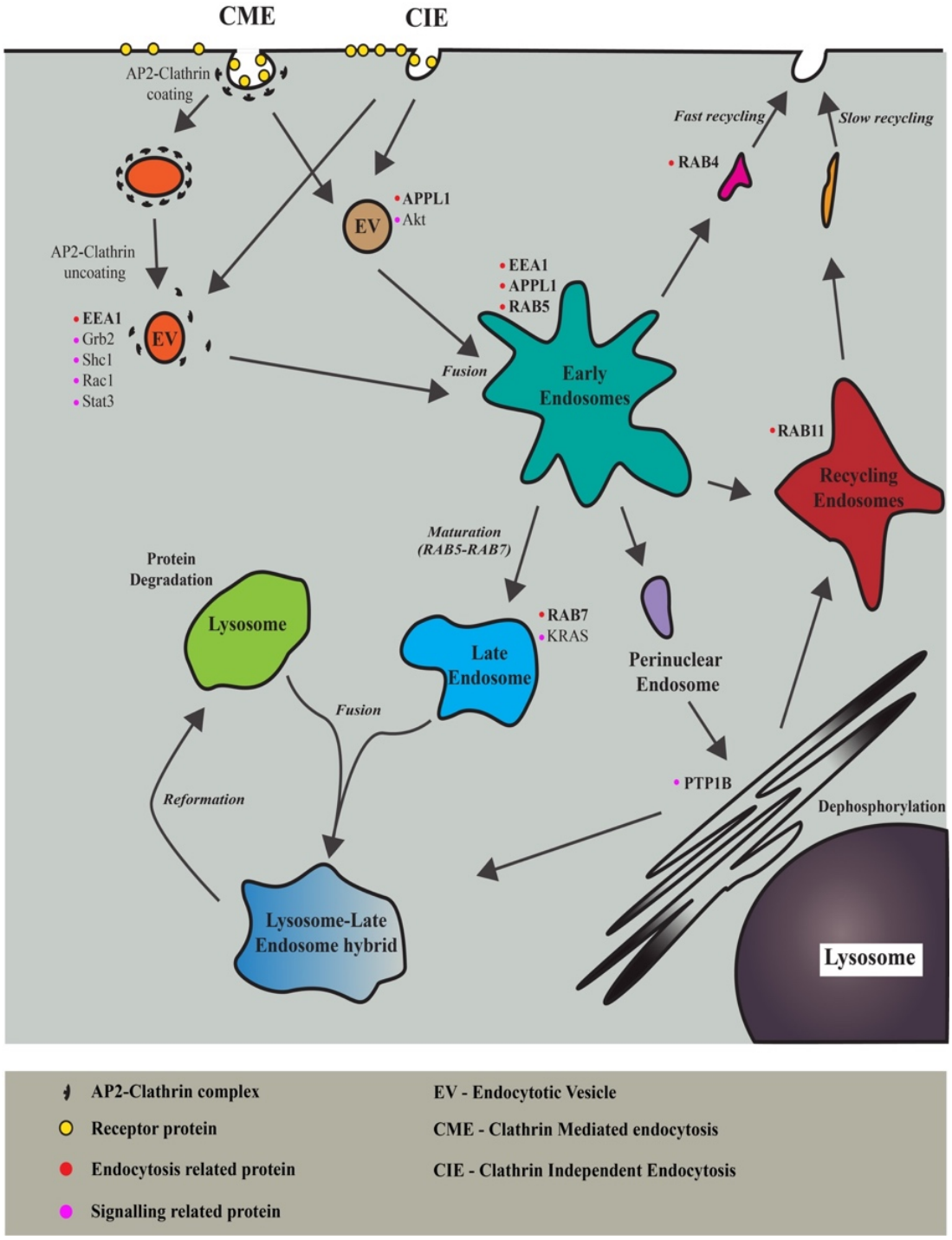

Figure 1-4 Vesicular trafficking of EGFR upon EGF stimulation. Ligand-bound EGFR is internalized and either recycled back to the PM via peripheral or pericentriolar recycling or targeted to lysosomes for degradation. The indicated Rab GTPases are specific for the different endosomal compartments and involved in endosomal fusion and fission events. Magenta-endosomal protein, Red-signaling protein

enzymes that degrades the EGFR signaling complex(Bucci et al., 1992; Rink et al., 2005). Ubiquitination mediated by cCbl is important to provide directionality to these vesicles to mature into the late endosomes(Ravid et al., 2004). A polyubiquitinated molecule is immune towards the activity of deubiquitinating enzymes (DUBs) present in the endosomal-sorting complexes required for transport (ESCRT) in the early endosomes(Millard and Wood, 2006). The de-ubiquitinated EGFR molecules are recycled back to the plasma membrane by Rab4 (fast recycling) or through perinuclear localized Rab11 positive endosomes (slow recycling) (Mohrmann et al., 2002; Ullrich et al., 1996).

Apart from endosomal sorting, presence of Rab7 positive late endosomes and Rab11 positive recycling endosomes in the phosphatase-rich perinuclear region plays an important role in spatial-temporal regulation of EGFR signaling. It has been shown that autonomously activated and ligand activated EGFR molecules employs different trafficking machinery. In absence of an external stimuli, spontaneous autocatalytic activation of receptors at the plasma membrane gets internalized and are recycled back after dephosphorylation at the recycling endosomes. Therefore, the primary function of EGFR recycling is to suppress spontaneous phosphorylation of Y845 that leads to autocatalysis. As the recycled species are predominantly monomeric, recycling of the receptor also maintains a specific receptor concentration at the plasma membrane allowing the cell to respond to ligand stimulation. Ligand activated EGFR molecules, on the other hand, gets ubiquitinated upon phosphorylation of tyrosine 1045 (Baumdick et al., 2015)and travels in unidirectional way to lysosomes through perinuclear region with high PTPN1/PTPN2 activity. As ligand binding stabilizes active conformation of EGFR that leads into sustained downstream signaling, unidirectional trafficking plays a major role in determining signal duration.

1.4 EGFR Regulation by Dephosphorylation

As ubiquination is directly dependent on phosphorylation of the tyrosine residues on EGFR to which cCbl binds, directly or via Grb2, dephosphorylation of these residues emerges as an important mechanism that affect EGFR trafficking(Grovdal et al., 2004; Parks and Ceresa, 2014). Similarly, the kinase activity as well as downstream signaling is affected

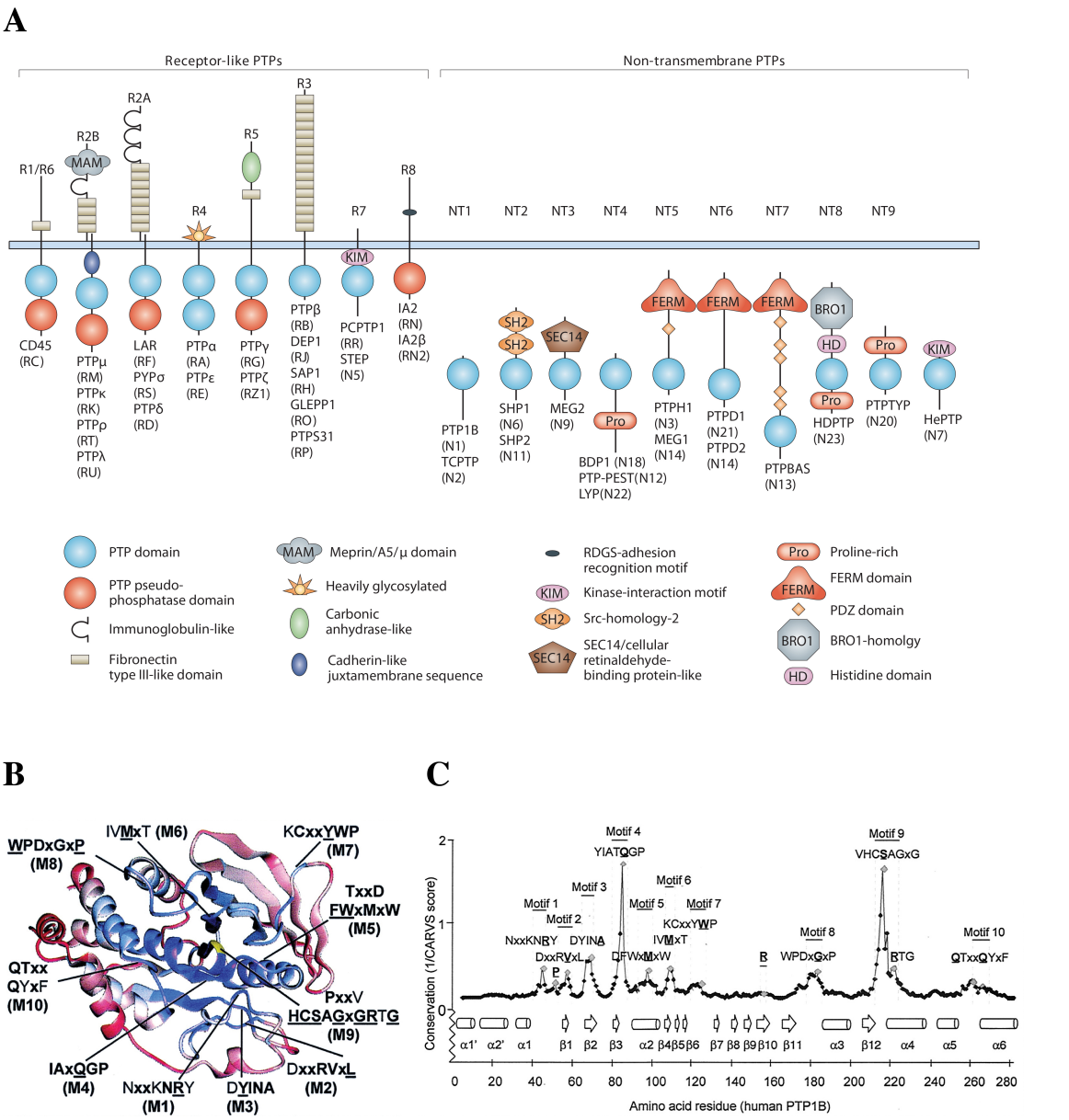

Figure 1-5 A) Structure of all the classical PTPs (Tonks, 2006). B) Representation of the catalytic domain of PTPN1 (Andersen et al., 2001) and B) details of different structural, catalytic and regulatory motif.

upon dephosphorylation of autocatalytic and signaling tyrosine residues, respectively. Dephosphorylation of pTyr residues of EGFR is carried out by a class of protein tyrosine phosphatase (PTP). There are 107 PTPs classified into different classes based on their homology in their PTP catalytic domain sequence(Andersen et al., 2001; Tonks, 2006). Classical PTPs are further classified as transmembrane receptor PTPs and non-transmembrane cytosolic PTPs (Figure 1-5).

Their differential activity on EGFR is an outcome of their enzymatic ability arising by their regulatory domain and oxidative potential of their compartment. Although the localization motif has no direct effect on the catalytic activity of the PTPs, which is confined to the active PTP domain, it controls the concentration in distinct spatial compartments and thus has an indirect effect on the role of the PTPs(Yang et al., 2007).

1.4.1 The PTP domain has highly conserved motifs

Apart from having an extra-cellular domain, a transmembrane domain and active PTP domain, few of the receptor-PTPs have an additional catalytically inactive PTP domain that is mostly involved in regulating in PTP activity. Some of the cytosolic PTPs, on the other hand, have adaptor domains like SH2, PEST in addition to a localization sequence.

PTP Domain

Upon sequence alignment of the PTP domains, ten conserved motifs obtained from PTP1B sequence were identified. (M1 to M10, Table 1-1).

Structural motifs (M2-M7): The hydrophobic segments assist in efficient packing of the protein structure assisting in its conformational stability.

Functional motifs (M1, M8-M10): PTP signature motif sequence (M9) present is involved in binding to the phosphate molecule of the substrate via the cysteine residue (a nucleophile).

The Arg and Ser residue in this motif are involved in stabilizing the thiolate form of the cysteine. With aromatic and non-polar amino acids in the sequence, M1 is involved in recognizing phosphotyrosine residues. As the sequence of the M1 motif is highly conserved among different PTPs (Table 1-1), it indicates a similar mechanism of substrate recognition.

Motif (residues in PTP1B)	Conservation	Conservation in 3D	Proposed roles of residues
Motif 1 40–46	NXXKNRY	Medium	pTyr-recognition motif: restricts substrate specificity to pTyr
Motif 2 53–59	DXXRVXL	Low	Structural motif: Hydrophobic core cluster
Motif 3 65–69	DYINA	Medium	Structural motif: Hydrophobic core structure. Tyr66, coordinates Asn44 through hydrogen bonding
Motif 4 82–87	IAXQGP	High	Structural motif: Assist in maintaining the PTP loop
Motif 5 91–101	TXXDFWXM XW	Medium	Structural motif: Contributes to form the conserved subdomain at the "back side"
Motif 6 107–111	IVMXT	Medium	Structural motif: Hydrophobic core cluster
Motif 7 120–126	KCXXYWP	Low	Structural motif: Hydrophobic core cluster
Motif 8 179–185	WPDXGXP	Low	Catalysis motif: The WPD loop that catalyxes the hydrolysis reaction (Trp179 & Pro180 - center of mediates motion of loop; Asp181 - general acid catalyst;
Motif 9 210–223	PXXVHCSA GXGRTG	High	Phosphate interaction motif: The Pro210, structural hydrophobic core; His214, lowers pKa of Cys215; Cys215, nucleophile; Ser216, H bonds with Tyr46 stabilizing its interaction with substrate; Ala217, phosphotyrosine binding, nonpolar interaction with substrate phenyl; Gly218, phosphotyrosine binding; Gly220, phosphotyrosine binding; Arg221, H bonds with phosphate oxygens [transition-state stabilization]; Thr222, lower pKa of Cys215
Motif 10 262–269	QTXXQYXF	Low	Catalysis motif: The Q loop that interacts with active site water molecule. Gln262 and Gln266 H bonds with scissile oxygen and active site water molecule.

Table 1-1 Details of different structural, catalytic and regulatory motif along with their sequences.

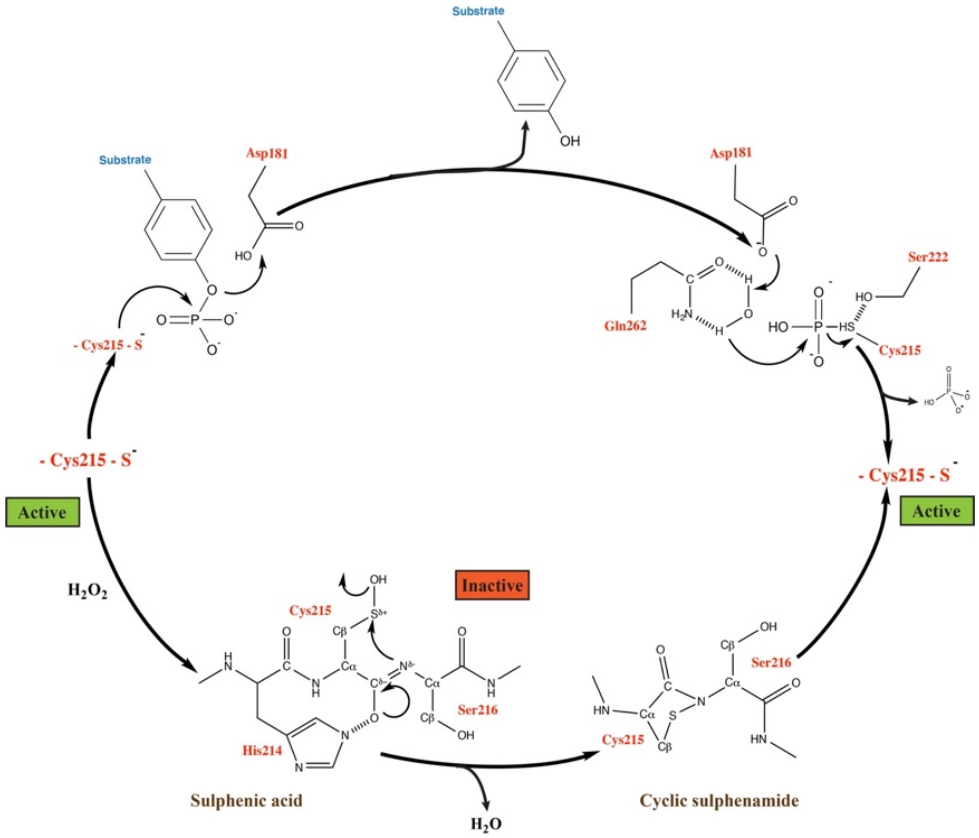

Figure 1-6 Schematic showing mechanism of Cys215 (PTPN1) mediated dephosphorylation of pTyr (Top) and reversible oxidation due to reactive oxygen species

The substrate binding leads to conformational changes that bring the WPD loop present in M8 close to the tyrosyl substrate and allows Asp (as a general acid catalyst) to donate a proton to the phenolate group. The Gln in M10 or catalytic-water motif assists in the second hydrolysis step of the phosphocysteine enzyme complex(Andersen et al., 2001).

Other Domains

The extracellular domain of many RPTPs are involved in a cell-cell interaction due to presence of Fibronectin type III-like, Meprin-A5 or Carbonic anhydrase like domains (Figure 1-5A). PTPRA and PTPRE are glycosylated at their N terminal which assists in their membrane localization(Tonks, 2006). Cytosolic PTPs, PTPN6/PTP11 and PTPN5/PTPN7, have the SH2 and KIM domain respectively that regulate their phosphatase activity(José et

al., 2003; Tenev et al., 1997). The FERM domain present in PTPN14 and PTPN21 mainly interacts with the endosomal proteins implying a possible function of these PTPs in endocytosis(Belle et al., 2015; Roda-Navarro and Bastiaens, 2014). PEST domain present in PTPN12 allows its substrate to be subjected to K3 proteasomal degradation; while the additional PTP domain in R-PTPs participates in regulating the phosphatase activity in an oxidizing environment(Yang et al., 2007).

1.4.2 Regulation

The SH2 domain, both in PTPN6 and PTPN11 interacts with the PTP domain and traps the protein in an auto-inhibited conformation(Sun et al., 2013). When the SH2 domain interacts with pTyr of an activated RTK, this releases the auto inhibition and elevates their phosphatase activity. Therefore, the dependency of these PTPs on their substrate for their activity is necessary in tuning EGFR activity. KIM domain of PTPN5/PTPN7 follows a similar mechanism with ERK as an interacting-activating partner(José et al., 2003).

The lower pKa value of the cysteine present in the PTP catalytic site makes it susceptible to oxidation(Weibrecht et al., 2007). Oxidative reactions occur mainly due to generation of reactive oxygen species (O_2^- or H_2O_2) by NOX complex triggered as a response to a stress or growth factor stimulation(Bánfi et al., 2003). Upon oxidation, the thiolate form of cysteine in the PTP loop is converted into sulfenic acid (intermediate) and is oxidized to sulfenamides(Ross et al., 2007). The sulfenic acid form of cysteine of the adjacent proteins can form a disulfide bond. Both sulfonamides and disulfide bonds can be readily reduced to thiols by the thioredoxin or glutathione-dependent systems. Depending upon the oxidative potential, the cysteine residue can also be irreversibly oxidized to sulfinic acids, sulfinamides, sulfonic acids or sulfonamides(Tanner et al., 2011).

Phosphorylation has also been pointed to be one of an important mechanism of PTP regulation. Tyr798 of PTPRA upon phosphorylation can act as a hub for Grb2 binding which might help in its internalization. The SH2 domain of SHP2 (upon phosphorylation of Tyr residues at the C terminal tail of SHP2) also acts a binding site for Grb2 which is necessary to maintain the SHP2 in an open conformation(Sun et al., 2013).

1.5 Interplay between EGFR and PTP activity

Previously, many screening experiments have been reported that presented PTPs as regulators of EGFR. A set of purified PTP proteins were screened for their activity on a peptide with an important pTyr residue specific to a particular RTK(Barr et al., 2009). These experiments showed that the EGFR pY1068 was a substrate for PTPN1, PTPN2, PTPN5,

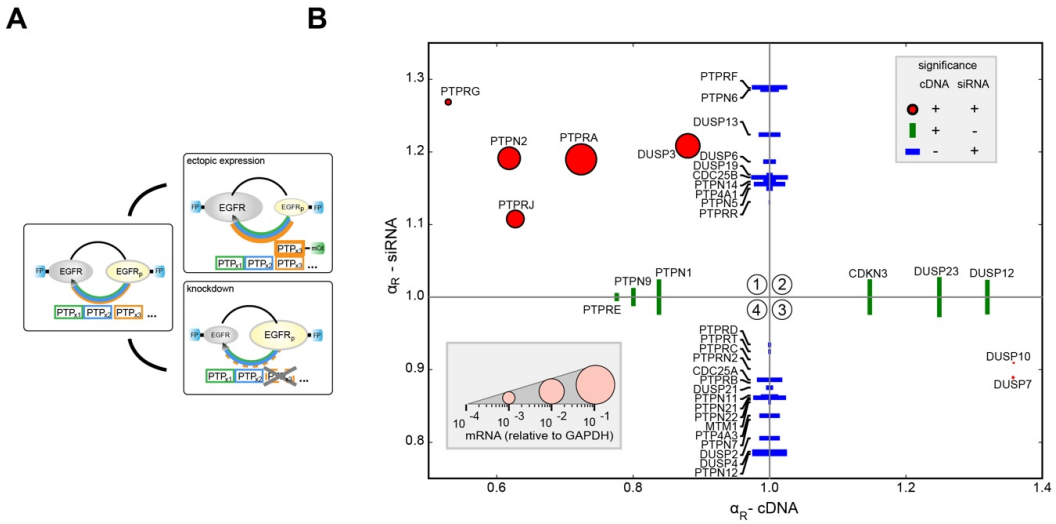

Figure 1- 7 Scatter plot of median EGFR phosphorylation fold-changes ($\boldsymbol{PFC_\alpha} = {}^{\alpha_{PTP}}/_{\alpha_{ctr}}$, n~150 cells per condition) upon siRNA-knockdown ($\boldsymbol{PFC_\alpha}$-siRNA) and ectopic PTPX-mCitrine expression ($\boldsymbol{PFC_\alpha}$-cDNA), 5min after 200ng/ml EGF stimulation. Significant $\boldsymbol{PFC_\alpha}$ upon both (red dots) or only one perturbation (green/blue lines, $p<0.05$) are shown. Marker length scaled to relative MCF7 PTP_X-mRNA levels.

PTPN9, PTPRA, PTPRB, PTPRC, PTPRE, PTPRG, PTPRJ and PTPRO. Among these, PTPRJ showed highest phosphatase activity. Another study with siRNA mediated PTP knockdown in MCF7 cells showed that PTPRJ and PTPRK act as negative regulators of EGFR(Tarcic et al., 2009). A recent PTP-EGFR interaction study, with a membrane two hybrid screen for Non-receptor PTPs and mammalian membrane two hybrid screen for Receptor PTPs, showed PTPN6, PTPN7, PTPN11, PTPN12, PTPRA, PTPRB, PTPRE, PTPRG, PTPRH, PTPRK, PTPRS, PTPRT, PTPRU and PTPRZ as interacting partner of EGFR(Yao et al., 2017). The same study also evaluated phosphatase activity of PTPRA, PTPRH and PTPRB towards EGFR.

Several PTPs were identified by cell array fluorescence lifetime imaging microscopy (CA-FLIM) to regulate ligand activated EGFR (Thesis-Fengler, 2014). siRNA mediated knock down or ectopic cDNA-mCitrine expression PTP in MCF7 cells with, identified PTPRG, PTPRA, PTPRJ, DUSP3 and PTPN2 as non-redundant negative regulators of EGFR. PTPN1, PTPN9 and PTPRE were identified as negative regulator of EGFR only in cDNA perturbation indicating that their activity might be redundant to other endogenous PTPs present in MCF7 cells. Other classical PTPs like PTPN5, PTPN6, PTPN14, PTPRF and PTPRR were identified in the siRNA screen implying either these proteins are regulated or they act on EGFR at later time points.

The phosphatase to kinase activity determines the phosphorylated state of EGFR. At the plasma membrane, PTP inhibition is coupled to the RTK activity via ROS generation (Reynolds et al., 2003). This double negative feedback topology between EGFR and PTP at the plasma membrane creates a bistable system (Reynolds et al., 2003). In general, a bistable system can switch between two distinct stable states. An EGF dosage that is able to bring the system above the bistable regime, can do so due to EGFR autocatalytic function attributed to pY845 phosphorylation coupled to PTP inhibition by ROS. With time,

internalized phosphorylated EGFR molecules encounter ER-PTPs with high phosphatase activity. This vesicular trafficking mediated negative feedback interaction brings down the total amount of phosphorylated EGFR and leads into shut down of the RTK signaling.

Although few PTPs have been identified as regulators of EGFR, the mechanism of regulation is still not clear. Characterizing the strength of each PTP activity on EGFR at different time point and determining if the regulation is direct or indirect will expand our understanding about PTP functionality. Phosphorylation at Y1045 of liganded EGFR causes ubiquitination and internalization leading it to lysosomes for degradation. With low degree of

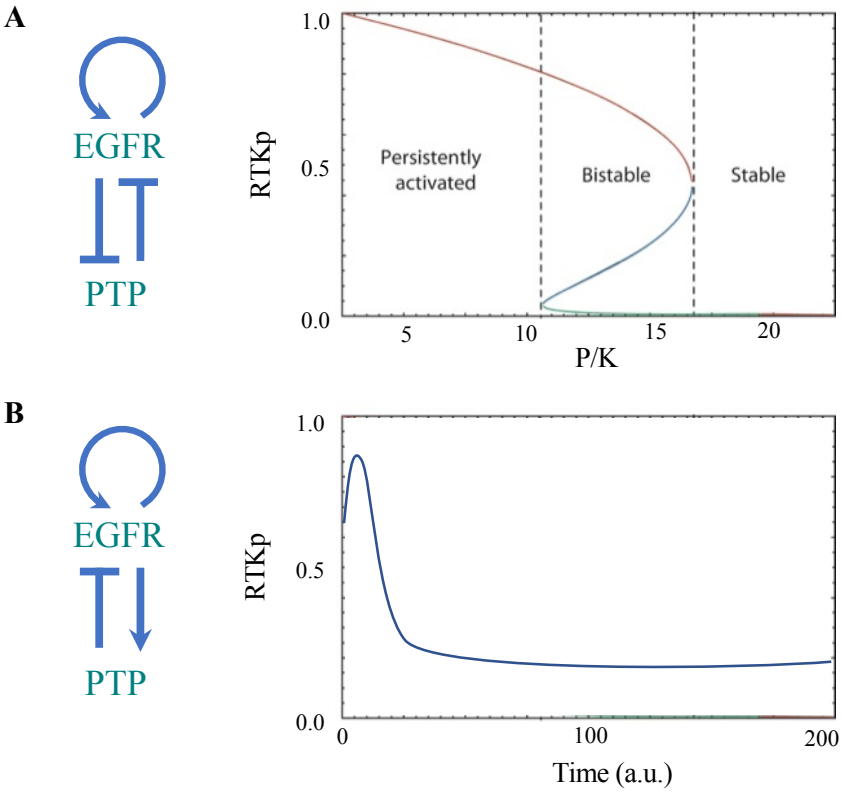

Figure 1-8 A) Schematic representation of the RTK – PTP network topology exemplifies a double negative feedback loop. Together with the autocatalytic activity of RTKs generates a bistable system. The fraction of phosphorylated RTK (RTKp) at steady state as function of the relative maximal PTP/RTK activity (P/K). Stable steady states (green line-resting; red line-activated), blue lines-unstable saddle point. Where the red and green lines coincide, the system is bistable (Reynolds et al., 2003) B) A negative feedback RTK–PTP interaction results in a single dynamical solution implying this interaction might play role in signal duration (Koseska and Bastiaens, 2017).

ubiquitination, monomeric EGFR is brought back to the plasma membrane through Rab11 recycling endosomes. The monomeric EGFR at the plasma membrane is able to maintain the responsiveness of a cell to varying EGF concentration, while liganded EGFR is mainly involved in downstream signaling via pY1068. How spatially distributed PTPs affect Y1045 and Y1068 phosphorylation will attribute to our understanding about how different PTPs affect EGFR response.

OBJECTIVES

In many cancer cells, elevated RTK activity results from loss or suppression of negative regulators i.e protein tyrosine phosphatase (PTP). Previous studies have shown that autocatalytic RTK activation is coupled to local PTP inhibition, thereby generating a bistable system exhibiting switch-like response properties (Reynolds et al., 2003;). Activated receptor molecules at the plasma membrane are rapidly endocytosed and traffic from early to late endosomes towards the lysosome. During vesicular trafficking, they interact with perinuclear-localized PTPs (e.g. PTPN1, which dephosphorylate activated receptors and thereby cease downstream signaling events. Although the significance of PTPs modulating EGFR activity and signaling has been described in numerous studies, it is still unclear how spatially segregated PTPs collectively regulate EGFR activity. Large-scale and individual studies have identified PTPs that regulate EGFR phosphorylation (Barr et al., 2009; Liu and Chernoff, 1997; Tarcic et al., 2009; Tiganis et al., 1998; Yao et al., 2017; Yuan et al., 2010). However, the functional role of individual spatially segregated PTPs in controlling the phosphorylation dynamics of EGFR remains unknown. In this thesis, quantitative imaging of EGFR phosphorylation in response to genetic perturbations of PTPs is employed to characterize the strength of the phosphatase activity of all PTPs which were identified as negative regulators during a reciprocal perturbation- CA-FLIM screen (Figure 1.7). By creating a library of PTP substrate-trapping mutants, we want to identify which PTPs are direct regulators of EGFR activity. With higher resolution microscopy techniques and single cell analysis, we aim to decompose the phosphorylation/dephosphorylation cycle of EGFR pY1068–Grb2 binding site, in space and time and create a spatial-temporal PTP reactivity map By determining the interaction and reactivity of PTPs over pre-stimulated and post 5P-EGF stimulated EGFR molecules, we want to identify PTPs that determine responsiveness of a cell to EGF stimuli and those that regulate signal duration.

2.1.1 CHEMICAL

Chemical	Manufacturer
2-Mercapto-ethanol	SERVA Electrophoresis GmbH
Acetic acid	Sigma-Aldrich
Ammonium persulfate (APS)	SERVA Electrophoresis GmbH
Ampicillin sodium salt	SERVA Electrophoresis GmbH
Bromophenolblue	Sigma-Aldrich
Copper(II) Sulfate ($CuSO_4$)	Sigma-Aldrich
Dimethyl sulfoxide (DMSO)	SERVA Electrophoresis GmbH
Dithiothreitol (DTT)	Fluka Analytical
Ethanol	J.T.Baker
Ethylenediaminetetracetic acid (EDTA)	Fluka® Analytical
Glycerol	GERBU Biotechnik GmbH
Hoechst 33342	Thermo Fisher Scientific
Isopropanol	J.T.Baker
Kanamycin sulfate	GERBU Biotechnik GmbH
Magnesium chloride ($MgCl_2$)	Merck KG/J.T.Baker
Methanol	AppliChem GmbH

N,N,N',N'-Tetramethylene-diamine (TEMED)	Sigma-Aldrich
Sodium chloride (NaCl)	Fluka Analytical
Sodium dodecyl sulfate (SDS)	SERVA Electrophoresis GmbH
Tris-base	Carl Roth GmbH
Tris-HCl	J.T.Baker
Tritox X-100	SERVA Electrophoresis GmbH
Tween 20	SERVA Electrophoresis GmbH
UltraPure™ Agarose	Thermo Fisher Scientific

2.1.2 EQUIPMENT

Centrifuge 5417 R (Eppendorf), Centrifuge 5810 R (Eppendorf), Concentrator plus (Eppendorf), Spectrophotometer (Beckman coulter), Master cycler (Eppendorf), Multiskan Ascent (Thermo E.C), Nanodrop ND-1000 (PeqLab), Gel Doc XR System (BioRad), Safe Imager (Invitrogen), Odyssey scanner (LiCor), Power Pac 300 (BioRad), Power Pac HC (BioRad), Vortexer (Scientific Industries), CO2 Incubator (IBS Integra), Biological safety cabinet (IBS Integra)

2.1.3 MEDIA

	Components
LB Media	10 g/l Bacto-Tryptone, 10 g/l Sodium chloride, 5 g/l Bacto-yeast extract
LB Media with Ampicillin	10 g/l Bacto-Tryptone, 10 g/l Sodium chloride, 5 g/l Bacto-yeast extract, 100 mg/l Ampicillin

LB Media plates with Ampicillin	10 g/l Bacto-Tryptone, 10 g/l Sodium chloride, 5 g/l Bacto-yeast extract, 100 mg/l Ampicillin, 1.5% Bacto-agar
TB Media	12 g/l Tryptone, 24 g/l Yeast Extract, 4 ml/l Glycerine, 0.17 M Monopotassium phosphate, 0.72 M Dipotassium phosphate
TB Media with Ampicillin	12 g/l Tryptone, 24 g/l Yeast Extract, 4 ml/l Glycerine, 0.17 M Monopotassium phosphate, 0.72 M Dipotassium phosphate, 100 mg/l Ampicillin
SOC Media	20 g/l Bacto-Tryptone, 5 g/l Yeast Extract, 0.58 g/l NaCl, 0.19 g/l CaCl2, 2.03 g/l MgCl2,6H2O, MgSO4, 7H2O, 2 % Glucose

COMMERCIAL MEDIA - CELL CULTURE

DMEM (P04-03600, PAN Biotech) with 10 % FBS, 1 % NEAA and 2 mM L-Glutamine (PAN Biotech), Non-essential amino acids 100x (PAN Biotech), Imaging media with Hepes (5961214, PanBiotech)

2.1.4 BUFFER

	Components
Separating Gel buffer	1 M Tris pH 8.8
Stacking Gel buffer	0.375 M Tris pH 6.8
Blotting Transfer Buffer	12 mM Tris, 96 mM Glycine pH 8.3, 20 % Ethanol
SDS-PAGE Running Buffer	25 mM Tris, 192 mM Glycine, 0.1 % SDS
TBS	100 mM Tris, 150 mM NaCL pH 7.6

TBST	100 mM Tris, 150 mM NaCL pH 7.6, 0.1 % Tween 20
5 x SDS sample Buffer	60 mM Tris-HCL ph 6.8, 25 % Glycerol, 2 % SDS, 14.4 mM Mercaptoethanol, 0.1 % bromophenolblue
1 x TAE Buffer	40 mM Tris, 20 mM Acetic acid, 1 mM EDTA pH 8.0
10 x DNA Gel loading Buffer	5 % Glycerol, 0.01 % OrangeG, 0.1 mM EDTA pH 7.54
SDS solution	10 % SDS in ddH2O
Ammonium Persulfate solution	5 % Ammonium persulfate in ddH2O
PBS-T	0.1 % Triton X100 in PBS (pH7.2)

COMMERCIAL BUFFERS/SOLUTIONS

NEB Buffer 2.1 (New England Biolabs), NEB Buffer 3 (New England Biolabs), 10X Lysis Buffer (Cell Signaling), Odyssey Blocking Buffer (Li-cor), Big Dye 5 x Buffer (Applied Biosystems), 5X Herculase II reaction Buffer (Agilent Technologies), T4 DNA Ligase Buffer (Invitrogen), Nuclease free water (Ambion), Premix Big Dye (Applied Biosystems), DPBS (P04-36500, PanBiotech), HistoFix (Roth).

2.1.5 ANTIBODIES

Goat anti-EGFR (AF231, R&D Systems**,** rabbit pY1045 (2237, Cell Signaling Technology**),** rabbit pY1068 (3777, Cell Signaling Technology), mouse anti-phosphotyrosine (PY72-P172.1, InVivo Biotech Services**),** anti-GAPDH (2118, Cell Signaling**),** IRDye 800 donkey anti-goat IgG (LI-COR Biosciences**),** IRDye 680 donkey anti-rabbit IgG (LI-COR Biosciences**),** Alexa Fluor® 568 donkey anti-mouse IgG (Life Technologies**),** Alexa Fluor® 568 donkey anti-mouse IgG (Life Technologies)

2.1.6 KITS

Roti®-Prep Plasmid MINI (Carl Roth GmbH), NucleoBond® Xtra Midi Plus EF (Macherey-Nagel), Micro BCA™ Protein Assay Kit (Thermo Scientific), Zymoclean™ Gel DNA Recovery Kit (Zymo Research), Herculase II Fusion Enzyme with dNTPs combo (Agilent Technologies), BigDye Terminator v1.1 cycle sequencing Kit (Applied Biosystems)

2.1.7 TRANSFECTION REAGENTS

FuGENE® HD Transfection Reagent (Promega), Lipofectamine® Transfection Reagent (Invitrogen), Dharmaffect1 (Dharmacon)

2.1.8 PLASMIDS AND OLIGOS

The p2297-OPIN(n)mCitrine (Berrow et al., 2007) and p2150-OPIN(c)mCitrine (Berrow et al., 2007) vectors without a His6-Tag were used as a backbone to generate the PTP_X–mCitrine library of expression constructs. PTP_X ORFs were cloned into p2297-OPIN(n)mCitrine or p2150-OPIN(c)mCitrine to obtain constructs with mCitrine to their N-terminus or C-terminus respectively. To obtain ORFs from human cell lines, mRNA was isolated with the RNeasy Maxi and Oligotex mRNA Midi Kit (QIAGEN) followed by cDNA synthesis using the AffinityScript Multiple Temperature cDNA Synthesis Kit (Agilent). The cloning of ORF into the pOPIN vector was done with a combination of 'in vivo cloning' (Oliner et al., 1993) and "sequence and ligase independent cloning (SLIC)" (Li and Elledge, 2007) by the Dortmund Protein Facility. The primers for ligation independent cloning (LIC) were designed with the help of the OligoPerfect primer designing and DNAstar lasergene tool of Invitrogen.

Table 2-1 contains a list of the PTP_X constructs along with mRNA reference ID, source of the cDNA/ORF, choice of the vector (C or N) and sequence of the Ligation-Independent-Cloning-(LIC) primers.

2.1.9 BACTERIAL CELL

Chemical competent XL 10 Gold bacteria cells were used for plasmid propagation.

2.1.10 MAMMALIAN CELLS

MCF 7 (human epithelial adenocarcinoma) were used for all the mammalian cell based studies

ENZYMES

Enzyme	**Company**
BglI	New England biolabs
Herculase II fusion DNA polymerase	Agilent Technologies
T4 DNA Polymerase	New england biolabs
Trypsin/EDTA	PanBiotech

2.1.11 DATABASE

DEPOD, UNIPROT, INSTRUCT were used to obtain information about the structure, localization and substrate

2.1.12 SOFTWARE

Lasergene DNA star, Matlab, Anaconda, Fiji, Prism, Chimera, Segmentor, EBI align, Expasy translate, OligoPerfect™ Designer

Gene name	expression vector	Source	LIC fwr Primer 5' - 3'	LIC rev Primer 5' - 3'
PTPRA	p2150-OPIN(c)mCitrine	cDNA from RT-PCR	TTACAATCAAAGGAGATATACCATGGATTCCTGGTTCATTCTTG	TGAAACAGAACTTCCAGAAACTTGAAGTTGGCATAATCTGAGAAT
PTPRE	p2150-OPIN(c)mCitrine	Biocat GmbH	AGGAGATATACCATGGAGCCCTTGTGTCCACTCCTG	AACAGAACTTCCAGAAATTTGAAATTAGCATAATCAGAAAATATATCAATAAAATCTTGTACCACTT
PTPRF	p2150-OPIN(c)mCitrine	Biocat GmbH	TTACAATCAAAGGAGATATACCATGGCCCCTGAGCCAGC	TGAAACAGAACTTCCAGAAACGTTGCATAGTGGTCAAAGCTGCC
PTPRG	p2150-OPIN(c)mCitrine	Biocat GmbH	AGGAGATATACCATGCGGAGGTTACTGGAACCGTGTTG	AACAGAACTTCCAGAAACACTAGGGACTCCATGCTCTCAGC
PTPRJ	p2150-OPIN(c)mCitrine	cDNA from RT-PCR	TTACAATCAAAGGAGATATACCATGAAGCCGGCGGCGCGGGAG	TGAAACAGAACTTCCAGAAAGGCGATGTAACCATTGGTCTTTCCAAATGTGGTCACGGGC
PTPN1	p2297-OPIN(n)mCitrine	Biocat GmbH	TGGAAGTTCTGTTTCAGGGTGAGATGGAAAAGGAGTTCGAG	TTAAACTGGTCTAGAAAGCTTTATGTGTTGCTGTTGAACAGGAAC
PTPN14	p2150-OPIN(c)mCitrine	Biocat GmbH	AGGAGATATACCATGCCTTTTGGTCTGAAGCTCCGCC	AACAGAACTTCCAGAAAAATGAGTCTGGAGTTTTGGAGGAACTG
PTPN2	p2297-OPIN(n)mCitrine	cDNA from RT-PCR	TGGAAGTTCTGTTTCAGGGTCCCACCACCATCGAGCGGGAG	TTAAACTGGTCTAGAAAGCTTTATAGGGCATTTTGCTGAAAAAACAGTGTCCAG

PTPN6	p2150-OPIN(c)mCitrine	cDNA from RT-PCR	TTACAATCAAAGGAGATATACCATGGTGAGGTGGTTTCACCGAGACCTCAG	TGAAACAGAACTTCCAGAAACTTCCTCTTGAGGGAACCCTTGCTC
DUSP10	p2150-OPIN(c)mCitrine	Biocat GmbH	AGGAGATATACC ATGCCTCCGTCTCCTTTAG ACGACAGG	AACAGAACTTCCAGAAA CACAACCGTCTCCACGCCC
DUSP7	p2150-OPIN(c)mCitrine	Biocat GmbH	AGGAGATATACC ATGCCCTGCAAGAGCGCCGA	AACAGAACTTCCAGAAA CGTGGACTCCAGCGTATTGAGTG
DUSP3	p2150-OPIN(c)mCitrine	Biocat GmbH	AGGAGATATACC ATGTCGGGCTCGTTCGAGCTCT	AACAGAACTTCCAGAAA GGGTTTCAACTTCCCCTCCTTGG
EGFR	p-mCherry N1 clontech			
EGFR	p-mCitrine N1 clontech			
EGFR	mTFP			
c-Cbl	TagBFP			
cDNA	**expression vector**	**mutation site**	**Mut fwr Primer 5' - 3'**	**Mut rev Primer 5' - 3'**
PTPN1	p2297-OPIN(n)mCitrine	D181A	CTATACCACATGGCCTGCCTTTGGAGTCCCTGAAT	ATTCAGGGACTCCAAAGGCAGGCCATGTGGTATAG
PTPN1	p2297-OPIN(n)mCitrine	C215S	GTT GTG GTG CAC AGC AGT GCA GGC ATC	GAT GCC TGC ACT GCT GTG CAC CAC AAC

PTPN14	p2150-OPIN(c)mCitrine	D1079A	TACTGACTGGCCAGCTCACGGCTGTCCAG	CTGGACAGCCGTGAGCTGGCCAGTCAGTA
PTPN2	p2297-OPIN(n)mCitrine	C216S	CCTGCGGTGATCCACAGTAGTGCAGGCATTG	CAATGCCTGCACTACTGTGGATCACCGCAGG
PTPN2	p2297-OPIN(n)mCitrine	D182A	ATTATACTACCTGGCCAGCTTTTGGAGTCCCTGAATC	GATTCAGGGACTCCAAAAGCTGGCCAGGTAGTATAAT
PTPN6	p2150-OPIN(c)mCitrine	C453S	CATCATCGTGCACAGCAGCGCCGGCAT	ATGCCGGCGCTGCTGTGCACGATGATG
PTPN9	p2150-OPIN(c)mCitrine	D470A	TCTTGAGCTGGCCAGCCTATGGTGTCCCTTC	GAAGGGACACCATAGGCTGGCCAGCTCAAGA
PTPRA	p2150-OPIN(c)mCitrine	C442S	CCATCGTGGTCCACAGCAGTGCAGGTGTA	TACACCTGCACTGCTGTGGACCACGATGG
PTPRE	p2150-OPIN(c)mCitrine	D250A	CAGTACTGGCCCGCCCAAGGCTGCTGG	CCAGCAGCCTTGGGCGGGCCAGTACTG
PTPRF	p2150-OPIN(c)mCitrine	D1507A	CATGGCCTGGCCAGCCCATGGAGTTCCTG	CAGGAACTCCATGGGCTGGCCAGGCCATG

PTPRG	p2150-OPIN(c)mCitrine	C1060S	CACACCAGCACTGCTGTGCACCAACACAG	CTGTGTTGGTGCACAGCAGTGCTGGTGTG
PTPRG	p2150-OPIN(c)mCitrine	D1028A	TACACAGTGGCCTGCCATGGGAGTTCCCG	CGGGAACTCCCATGGCAGGCCACTGTGTA
PTPRJ	p2150-OPIN(c)mCitrine	D1205A	CCTCCTGGCCAGCCCACGGTGTTCC	GGAACACCGTGGGCTGGCCAGGAGG

Table 2-1 List of all the plasmids used for different experiments

2.2.1 GENERATING PTP TRAPPING MUTANTS

To determine if PTPx directly interacts with EGFR, the catalytic site of PTPs were mutated. The site of mutation was chosen on the basis of WPD and XHCSAGXG motif in the active PTP domain(Andersen et al., 2001). The forward and reverse mutagenesis primers were designed using the DNA Star Lasergene software. The PCR reaction comprised of LIC primers and Phusion Flash High-Fidelity PCR Master Mix (Thermo Fisher Scientific) or Herculase II Fusion DNA Polymerase (Agilent). All PTP_x-pOPIN sequences were evaluated by using BigDye® Terminator v3.1 Cycle Sequencing Kit (Thermo Scientific). The plasmids were extracted from transformed E.coli XL - 10 Gold ultracompetent cells using a high content NucleoBond® Xtra Midi EF (Macherey-Nagel) according to the manufacturer's protocol. The site of mutation, sequences of the LIC and mutagenesis primers are listed in (Table 2.1).

POLYMERASE CHAIN REACTION

Mutation was introduced into the WT PTP_X cDNA by an overlap extension PCR and was later cloned into their respective plasmid backbone by using LIC strategy. Herculase II fusion DNA polymerase was used along with dNTPs and 5x Herculase buffer obtained from the Herculase kit (Agilent Technologies). A calculated amount of DNA was added to the reaction mix with 10 µM of designed primers. To optimize the PCR reaction different DMSO concentrations were used. All volumes of the components for the reaction mix are listed in

Component	Volume
5 x Herculase II reaction Buffer	10 µl
25 mM dNTPs	1 µl
Herculase II fusion DNA polymerase	1 µl
Primer forward	1.25 µl

Primer reverse	1.25 µl
50 ng plasmid DNA	0.33 µl
DMSO 0 / 3 / 6 / 8 %	0 / 1.5 / 3 / 4 µl
dd water	X µl to final 50 µl volume

The Mastercycler (Eppendorf) was used with a thermal cycle program as described in following Table. A 2-step PCR protocol was used wherein the first cycle governs association and amplification of the cDNA through its complimentary part of the LIC primers. The second cycle fuses the two PCR products.

	Temperature	Time	Cycle
Initialization	98 °C	1 min	1 X
Denaturation	95 °C	20 sec	3 X
Annealing	50.1 °C	20 sec	3 X
Extension	72 °C	45 sec	3 X
Denaturation	95 °C	20 sec	30 X
Annealing	58.8 °C	20 sec	30 X
Extension	72 °C	45 sec	30 X
Final extension	72 °C	1 min	1 X
Hold	8 °C		

SEPARATION AND PURIFICATION OF THE PCR PRODUCT

PCR products were separated using electrophoresis in a 1.0 % agarose gel for 45 min at 120 V. Furthermore, RedSafe, a DNA binding dye was added at a concentration of 50µl/l to detect the PCR product. Also, 10 µl

2log ladder was loaded to the gel. The band with the expected size was cut out of the gel with help of the Safe imager (Invitrogen). The PCR product was purified by Zymoclean Gel DNA recovery kit and the concentration was measured with help of the Nanodrop at 260 nm.

LIGATION

To create 5' overhang the PCR product and RE site cut pOPINE vector was incubated with the T4 DNA Polymerase. The components of the reaction mix are listed in the following table.

Components	Volume
10 X NEB2 Buffer	2 µl
T4 DNA Polymerase	0.2 µl
100X BSA	0.2 µl
Insert	9 µl
dd water	add to 20 µl

The mixtures were incubated for 1 h at 22 °C and later the enzyme was heat inactivated at 75 °C for 20 min. The pOPINE vector was also incubated with this polymerase to create similar single-strand 5' overhang. The concentration of T4 DNA polymerase treated PCR product and vector was determined. Two different ratios of vector to insert were used; 1:1 and 1:2. For calculating the quantity of the insert, the following equation was used:

$$concentration\ Insert\ DNA\ [ng] = \frac{Vector\ conc.\ [ng] \cdot Insert\ size\ [bp]}{Vector\ size\ [bp]}$$

The reaction mix was incubated for 30 min at 37 °C with 1X T4 DNA Ligase Buffer.

After the annealing reaction, 5 µl of the reaction mix was used for transformation into chemical competent *E. coli* cells that complete the assembly by recombination.

TRANSFORMATION

Aliquots of 45 µl XL10-Gold (Stratagen) or SCS-110 Stratagen) chemical-competent cells were thawed on ice and mixed with 2 µl β-Mercapto-ethanol (SERVA Electrophoresis GmbH). The mixture was incubated for 10 min on ice. After incubation, 2 µl DpnI digested PCR product was added and cells were incubated for 30 min on ice. Cells were heat-shocked at 42°C for 30 s and placed back on ice for 2 min. 500 µl SOC medium was added cells were incubate for 1 h under moving at 37°C. Cells were shortly centrifuged down and most of the medium removed. Cells were resuspended in the remaining medium and plated on an agarose/LB plate containing Ampicillin. Plates were incubated over night at 37°C. On the next day, single colonies were selected and incubated in 5 ml LB containing 100 µg/ml Amp. Single clone cultures were incubated over night at 37 °C under moving.

Isolation and purification of Plasmid DNA

The aforementioned overnight culture was used for plasmid isolation using the Roti-Prep Plasmid Kit from Roth. All steps were performed as outlined in the manual. For elution of the plasmid DNA from the silica gel membrane, 30 µl of warm nuclease free water was used. Furthermore, these overnight cultures were needed for plasmid DNA purification. The overnight culture of the transfected XL10 Gold *E. coli* cells was transferred to a flask containing 250 ml TB media for growing a second overnight culture of the *E. coli* cells. The next day the optical density was measured at 600 nm for adjusting the cell mass and culture volumes for high-copy plasmids purification. All following purifications steps were performed with the Endotoxin-free plasmid DNA purification Kit (Macherey Nagel). For the reconstitution of the plasmids 200 µl nuclease free water was used, afterwards the concentration was determined with the Nanodrop.

Restriction control of the plasmid

For a first indication whether the insert and vector were ligated correctly, the plasmid DNA was cut into pieces using restriction enzymes, which cleaved the plasmid at specific palindromic sequences. The control vector exhibits a defined amount of restriction enzyme sites. The ligation of insert and vector can influence the amount of restriction enzyme sites so as to change the size of the cut plasmid sequences. For this control, the restriction enzyme BglI form NEB was used. The reaction mix was prepared and incubated for 2 h at 37 °C. For

inactivation of the enzyme an incubation time of 20 min at 65 °C was chosen. Afterwards, the cut plasmid sequences were separated in an agarose gel.

Components	Volume
3.1 NEBuffer	5 µl
Restiction BglI enzyme	1 µl
Plasmid	1 µg
dd water	add to 50 µl

SEQUENCING

The BigDye Terminator v1.1 cycle sequencing Kit was utilized for performing fluorescence-based cycle sequencing reactions. This method is based on the Sanger sequencing also called dye-terminator sequencing that can be performed in one reaction. The buffers remaining from this kit contained all required components for the sequencing reaction. This buffer contains the polymerase and the dNTPs as well as four version of ddNTP-dye conjugates.

Components	Volume
Premix BigDye	2 µl
5x Buffer	3 µl
Primer	0.5 µl
DNA	x µl
dd water	add to 20 µl

In this type of PCR reaction the polymerase extends the DNA strand by addition of unmodified dNTPs. The reaction stops when the labeled dideoxynucleotide gets introduced into the strand. After the PCR, the products

are purified with the Nucelo colums Kit. The samples are then dried for 1 hour at 60 °C in a vacuum. With the help of electrophoresis procedure, the amplified strands with distinct length get separated. Afterwards the intensities of the labeled dideoxynucleotides for each position can be measured so that a chromatogram of the sequence could be established.

Temperature	Time	Cycle
96 ˚C	1 min	
96 ˚C	10 sec	25x
50 ˚C	5 sec	25x
60 ˚C	4 min	25x
hold 4 ˚C		

2.2.2 CELL CULTURE

MCF-7 cells (ECACC, Cat. No. 86012803) were cultured in Dulbecco's modified Eagle's medium (DMEM) (PAN Biotech), supplemented with 10% heat-inactivated fetal calf serum (FCS) (PAN Biotech), 10mM glutamine (PAN Biotech), 1% Non-Essential Amino Acids (PAN Biotech), 100U/ml penicillin (Gibco) and 100U/ml streptomycin (Gibco) at 37ºC with 5% CO_2. MCF7 cells were authenticated by Short Tandem Repeat (STR) analysis (Leibniz-Institut DSMZ). Cells were regularly tested for mycoplasma contamination using MycoAlert Mycoplasma detection kit (Lonza).

2.2.3 MRNA PROFILING

MCF7 cells were trypsinized and $6x10^5$ cells were suspended in 4ml RNAse free water (Thermo Scientific) with 1ml RNA Later (Thermo Scientific). mRNA extraction and profiling was performed by Comprehensive Biomarker Center GmbH, Heidelberg on an array designed by Agilent 60-mer Sure print technology. The mRNA levels were obtained from three independent runs.

2.2.4 TRANSFECTION

$3x10^4$ MCF7 cells were seeded per well in an 8-well Lab-Tek chamber (Nunc). After 7-8 h of seeding, cells were transfected with 0.125µg of each plasmid (EGFR-mTFP, PTP_X-mCitrine or cCBL-BFP) by using FUGENE6 (Roche Diagnostics). The cells were incubated along with the transfection mixture overnight at 37°C with 5% CO_2. Before EGF stimulation, cells were growth factor starved with supplemented DMEM (see above) without FCS for 6h. The cells were stimulated with a sustained or a 5min-pulse of 200ng/ml EGF-Alexa647. Cells were chemically fixed with Roti® Histofix 4% (Carl Roth) for 20 min, washed three times with PBS and then permeabilized with 0.1% Triton-X/PBS (SERVA Electrophoresis) for 15min. Cells were stored with PBS at 4°C before immunostaining. For the siRNA mediated knockdown experiments, 2×10^4 of MCF7 cells were seeded in each well of an 8-well Labtek dish and were transfected after 24h using 50nM siRNA specific for PTPN2, PTPRG, PTPRJ or non-targeting control siRNA with Dharmafect1 according to the manufacturer's instructions.

2.2.5 siRNA CONCENTRATION OPTIMIZATION FOR THE KNOCK-DOWN EXPERIMENTS

2×10^5 of MCF7 cells were seeded in each well of a 6-well tissue culture dish and transfected after 24h using 50nM siRNA specific for PTPN2, PTPRG, PTPRJ, or non-targeting control siRNA with Dharmafect1 according to the manufacturer's instructions. RNA was isolated 24h after transfection using the Quick-RNA MicroPrep kit (Zymo Research, Freiburg, Germany). For quantification of the mRNA expression levels of interest, 1µg of the isolated RNA was used for reverse transcription using the High Capacity Reverse Transcription kit (Applied Biosystems) according to the manufacturer instructions. Commercially available TaqMan assays (Thermo Fisher), PTPN2(Hs00959888_g1), PTPRG(Hs00892788_m1), PTPRJ(Hs01119326_m1), GAPDH(Hs02786624_g1), CYBA(Hs00609145_m1) were used to detect the amplicons after each cycle of a qPCR reaction ran in an IQ5 real-time PCR system cycler (Bio-Rad). Cycling condition were as follows: 40 cycles of 95°C for 10s and 57°C for 30s. Data were analyzed using the ΔΔCt method for determination of relative gene expression by normalization to an internal control gene (GAPDH), and fold expression change was determined compared to the control siRNA sample.

2.2.6 PROTEIN AND PEPTIDE CONJUGATION REACTION

hEGF-ALEXA647

His-CBD-Intein-(Cys)-hEGF-(Cys) plasmid (Sonntag et al., 2014) was kindly provided by Prof. Luc Brunsveld, University of Technology, Eindhoven. Human EGF was purified from E. coli BL21 (DE3) and was labelled at its N terminus with Alexa647-maleimide as previously described(Sonntag et al., 2014). Labelled EGF-Alexa647 was stored in PBS at -20°C.

PY72-Cy3.5 LABELLING

Cy3.5® NHS ester (GE Healthcare) was dissolved in 10µl of dried N,N dimethylformamide (SERVA Electrophoresis). For each reaction, 15µl of 1 M Bicine (pH 9.0) and 10-fold molar excess (to PY72) of Cy3.5 was added to 100µl PY72 (0.25mg/ml) in PBS. The reaction was allowed for 20min in the dark and was terminated by adding 6µl of 0.2M Tris buffer (pH 6.8). Free dye was removed by using 7K Zeba Spin Desalting Columns (Thermo Scientific). The absorption (A) of the filtrate was measured at 280nm (PY72) and 581nm (Cy3.5). For immunostaining, labelled antibody (30µg/ml in PBS) with dye to protein ratio of 3 - 5 was used.

$$\left(\frac{Dye}{Protein} = \frac{A581 * 1.7}{(A280 - 0.24 * A581) * 1.5}\right)$$

2.2.7 HIGH-CONTENT SCREENING

After 12-14 hours of transfection, cells were starved for 6 hours (DMEM 0 % FCS) and stimulated with 200 ng/ml EGF for indicated times according to the experiment. The stimulus was removed after the first 5 min and replaced by starving medium. Cells were chemically fixed with 4 % PFA/PBS (Sigma-Aldrich) for 20min. Cells were washed 3x with TBS and 10 min permeabilized with 0.1 % Triton-X/PBS (SERVA Electrophoresis GmbH). Afterwards, cells were stained for 10 min with 0.5 ng/ml Hoechst (Molecular Probes). The 8-well dish were placed on a metal stage holder and fixed with superglue. After calibrating the system, every center position of each well was focused and saved (2 positions per well). A grid of 5x5 subpositions was chosen that used the saved position as a center and acquired 25 images around it. At every subposition, the sample plane was auto-focused in the Hoechst channel. Fluorescent images and FLIM-stacks were acquired at each subposition before and after addition of the FRET acceptor (anti-pY-Cy3.5).

2.2.8 TRAPPING MUTANT FLIM

Confocal FLIM experiments were performed using a time-correlated single-photon counting module (LSM Upgrade Kit, PicoQuant) on an Olympus FV1000 confocal microscope (see: Confocal microscopy). Pulsed lasers were controlled with the Sepia II software (PicoQuant) at a pulse repetition frequency of 40MHz. The

sample was excited using a 440nm diode laser (LDH 440, PicoQuant). Fluorescence emission was spectrally filtered using a narrow-band emission filter (HQ 480/20, Chroma). Photons were detected using a single-photon counting avalanche photodiode (PDM Series, MPD, PicoQuant) and timed using a single-photon counting module (PicoHarp 300, PicoQuant). Using the SymPhoTime software V5.13 (PicoQuant), images were collected after an integration time of ~ 4min collecting ~ 3.0–5.0x10^6 photons. For each pixel, the single photon arrival times of the TCSPC measurement were used to calculate the complex Fourier coefficients of the first harmonic and were corrected by the Fourier coefficient of a calculated reference (Grecco et al., 2010).

2.2.9 Immunofluorescence imaging

Permeabilized cells were incubated with 200µl of Odyssey Blocking buffer (LI-COR) for 30min. All the antibodies were diluted in Odyssey Blocking buffer (LI-COR). Primary antibodies were applied for 1h and fluorescently tagged (Alexa568) secondary antibodies for 30min. Cells were washed three times with PBS between each antibody incubation step. Cells were imaged in PBS at 37°C. The Olympus FluoView FV1000 confocal microscope was equipped with a temperature-controlled CO_2 incubation chamber at 37˚C and a 60x/1.35 NA Oil UPLSApo objective (Olympus Life Science). Fluorescent fusion proteins with BFP, mTFP and mCitrine were excited using the 405nm Diode-UV laser (FV5-LD05, Hatagaya) and the 458/488nm lines of an Argon-laser (GLG 3135, Showa Optronics). Cy3.5/Alexa568 were excited with a 561nm DPSS laser (85-YCA-020-230, Melles Griot) and Alexa647 was excited with a 633nm He-Ne laser (05LHP-991, Melles Griot). Detection of fluorescence emission was restricted with an Acousto-Optical Beam Splitter (AOBS): BFP (425-450nm), mTFP (472-502nm), mCitrine (525-555nm), Cy3.5/Alexa568 (572-600nm), Alexa647 (655-755nm). Scanning was performed in frame-by-frame sequential mode with 3x frame averaging and a pinhole of 2.5 airy units.

2.2.10 Quantification and Statistical Analysis

Global analysis of FLIM data

The global analysis of FLIM data uses the whole image (=global) set to extrapolate the decay rate of the donor molecules without (D) and with an acceptor molecule (DA). That then uses the information in each pixel of an image to determine the fraction of donor molecules (EGFR-FP) interacting with an acceptor molecule.

If we have two different lifetimes from donor only molecules and donor molecules interacting with acceptor molecules in a certain configuration, the fraction (α) of interacting molecules within each pixel can be calculated according to:

$$\alpha(x,y) = \frac{\tau_{DA} A_{DA}(x,y)}{\tau_D A_D(x,y) + \tau_{DA} A_{DA}(x,y)}$$

where A_D is the amplitude of the donor only molecules and A_{DA} the amplitude of the acceptor-bound donor molecules and τ_D and τ_{DA} are the corresponding lifetimes.

For global analysis, the single photon arrival times of the TCSPC measurement for each pixel were used to calculate the complex Fourier coefficients of the first harmonic (Grecco et al., 2009). In a second step the Fourier coefficients were corrected by the Fourier coefficient of a calculated reference. The corrected Fourier coefficients are then plotted into a phasor plot, so that the Fourier coefficients from each pixel of the image set are represented by one point in the phasor plot (Figure 2-2-1).

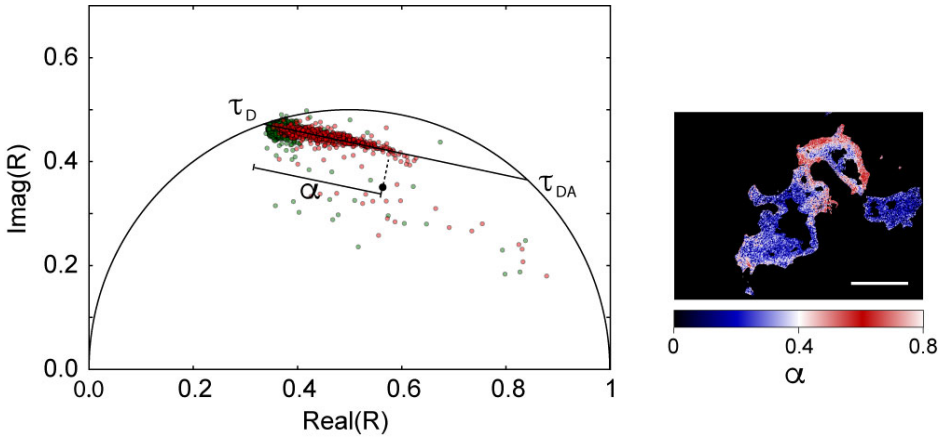

Figure 2-2-1 Phasor plot showing a linear fit of the fluorescence emission Fourier coefficients (R) in the complex plane yielding the global lifetimes in presence (τ_{DA}) and absence (τ_D) of FRET. Fraction of donor molecules interacting with the acceptor (α) in each pixel was calculated from the projection onto the τ_D-τ_{DA} line segment. An exemplary spatially resolved α-map (right) are shown. Scale bar: 20µm.

By fitting a straight line through all points in the phasor plot, the "global lifetimes" τ_D and τ_{DA} are determined at the intersections with the half-circle. τ_{DA} is the donor fluorescence lifetime in presence of the acceptor and τ_D the donor-only lifetime. Finally, the projection of each point in the phasor plot into the fitted segment between τ_D and τ_{DA} can be used to calculate the relative fraction of donor-only and donor-acceptor pairs (α) in each pixel.

SINGLE CELL SEGMENTATION AND QUANTIFICATION

Cells were segmented in CellProfiler (Kamentsky et al., 2011) using the image of the nuclear stain (Hoechst) and EGFR-mTFP. All images were corrected for background and bleed through, and mean values per cell (excluding the nuclear region) from all channels were obtained. To match the images of the FLIM MCP and the high-resolution CCD camera, the masks were affine transformed (OpenCV).

PTP SPECIFIC REACTIVITY

The α_{median} of each cell was plotted against the respective PTP_X–mCitrine mean intensity per cell for each time point. If the distributions of $\alpha_{median,\ PTPx}$ and $\alpha_{median,\ ctr}$ were significantly different (Mann–Whitney U, $p<0.05$), the data was fitted with an exponential function ($\alpha = c + A \cdot e^{-k \cdot PTPx}$). For each time point, the cells of the respective control measurement were included in the fit after removing outliers (± 3x median absolute deviation around the median). The control coefficient that reflects the dephosphorylating efficiency of each PTP_X was determined from the slope of the exponential function at 0 calculated from –k*A, where k is the rate and A is the amplitude. For weak α - PTP_X-mCitrine intensity dependencies, the control coefficients were determined from the slope of a linear fit.

SPATIAL-TEMPORAL MAPS (STMS)

Cells were masked from the EGFR images using FIJI (https://fiji.sc/), the nuclei were segmented using CellProfiler from the nuclear stain (Hoechst) or cCBL-BFP images. The distribution of observables or derived quantities in cell was determined by obtaining radial profile upon single cell analysis by using Python based Segmentor tool developed by Dr Klaus Schuermann.

For each pixel within the cell, the distance to the closest PM and nuclear membrane (NM) were calculated to derive a normalized distance $r = r_{PM} / (r_{PM} + r_{NM})$. All pixels were split in 10 intervals according to their

normalized distances. For each of the observables (EGFR-mTFP, PTP_X-mCitrine, pY_i-Alexa568, and EGF-Alexa647 fluorescence intensities) or derived quantities (α, pY_i-Alexa568/ EGFR-mTFP, EGF-Alexa647/ EGFR-mTFP, PFC), the mean value was calculated for each segment, yielding a radial profile for the individual cells. To calculate the radial distribution of EGFR-mTFP phosphorylation at distinct pY_i sites, the mean fluorescence per segment of the pY_i channel was divided by the corresponding mean EGFR-mTFP fluorescence. With the exception of α and pY_i/EGFR-mTFP images, all profiles were divided by the total cell mean and an average radial profile was calculated. The radial profiles from the distinct time points were then combined to yield the corresponding spatial-temporal maps. Cells in which PTP_X-mCitrine expression levels saturated EGFR dephosphorylation were excluded from the analysis (Fig. S4b, explanation below).

The STM of the phosphorylation fold-change (PFC) was calculated by dividing the STM pY_i /EGFR-mTFP of the control by the STM pY_i/EGFR-mTFP for each PTP_X-mCitrine. The profiles from multiple experiments were averaged and significance was determined using $k \sum_{i=0}^{n-1} \frac{(-\ln(k))^i}{i!}$, where $k = \prod_n p_i$, and p_i denotes the individual p-values from a Student's t-test comparing the pY_i /EGFR-mTFP distributions of the control to that upon the respective PTP_X-mCitrine expression at each point in space and time.

3.1 DETERMINING EGFR-PTP INTERACTION

In order to evaluate if the PTPs identified in the reciprocal perturbation screening are direct negative regulators of EGFR, PTP-mCitrine trapping mutants (TM) were generated by modifying the catalytic site Cysteine to Serine (C/S), Aspartate to Alanine (D/A) or C/S with D/A (Double mutants-DM)(Blanchetot et al., 2005; Flint et al., 1997). To assess the interaction between PTPx-mCitrine and EGFR-mTFP, we used a FRET-FLIM approach where mTFP that is tagged to EGFR acts as a donor and mCitrine tagged to PTPx acts as an acceptor. The MCF7 cells ectopically expressing PTP_X^{TM}-mCitrine and EGFR-mTFP were stimulated with 5 min pulse (5P) of 200ng EGF, which allowed identifying PTPs that interact with ligandless EGFR and liganded EGFR.

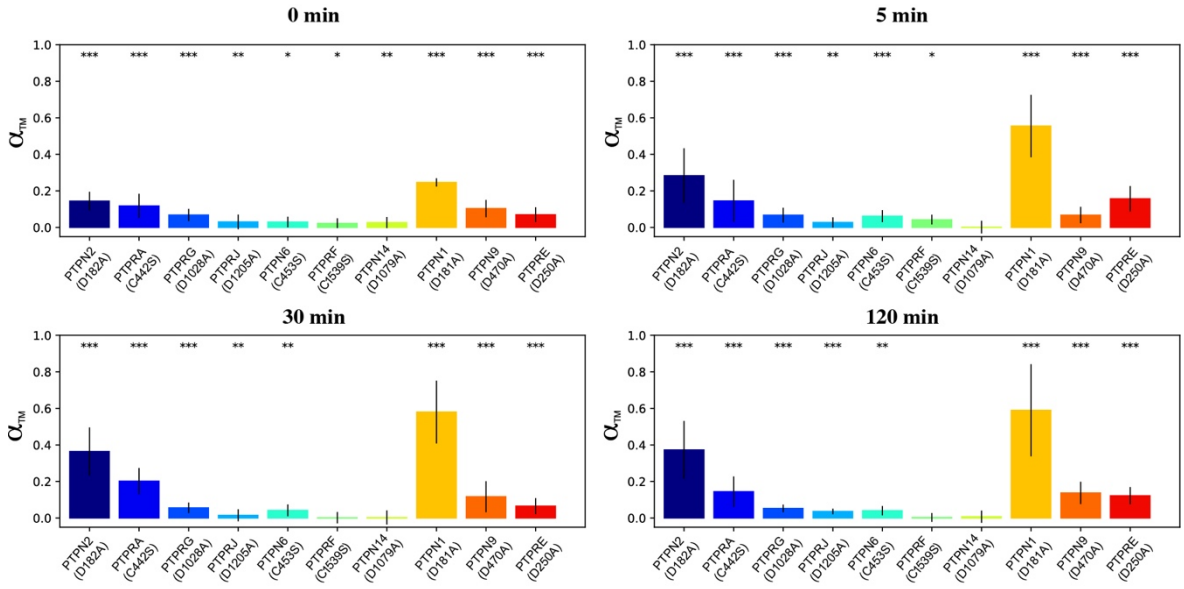

Figure 3-1 Average fraction of EGFR-mTFP interacting with catalytically impaired PTP_X-mCitrine trapping mutants (α_{TM} ± SD, n=15-20 cells, * p<0.05, ** p<0.01 and *** p<0.001). MCF7 cells ectopically expressing $PTPx^{TM}$ –mCitrine and EGFR-mTFP were stimulated with 5P-200ng EGF for 30min and 120 min time point.

Out of various trapping mutant versions of each of the PTPs, i.e C/S, D/A and DM, only those mutants that showed strongest interaction are represented (Figure 3-1). PTPN1/2/9 and PTPRA/E/G strongly interact with unstimulated EGFR implying that these PTPs have a potential to act on the ligandless autonomously activated EGFR and play an important role in its safeguard mechanism (Baumdick et al., 2015). The interaction of ER-PTPs is stronger as compared to the R-PTPs, due to various factors. First, there is a structural difference in the catalyitc site of ER-PTPs, cyt-PTPs and R-PTPs. Unlike ER-PTP, binding of cyt-PTPs and R-PTP to its substrate is determined by both their catalytic sites and other domains that affect the efficiency of these PTPs towards their similar substrate (Sarmiento et al., 2000). Upon stimulation, all PTPs except PTPRG showed an increase in interaction with liganded EGFR. PTPRA on the other hand showed an increase in interaction only at late time points which indicates some kind of regulation that inhibits its binding to the substrate at early time points. The interaction also depends on the spatial localization of the PTPs which determines the substrate accessibility. The increase in interaction of EGFR to ER- bound PTPN1/N2 can be only availed by vesicular trafficking as it is a primary mode through which an interaction between ER localized-PTP and plasma membrane localized EGFR can be accomplished, making it an important part of the EGFR phosphorylation-dephosphorylation cycle (Baumdick et al., 2015).

3.2 Regulation of the temporal EGFR phosphorylation profile by PTPs

The reciprocal perturbations (Figure 1-7) singled out the non-redundant PTPs and implied the direct regulators of EGFR on the basis of siRNA and cDNA perturbation, respectively. While the interaction studies showed which and when these PTPs interact with EGFR, the

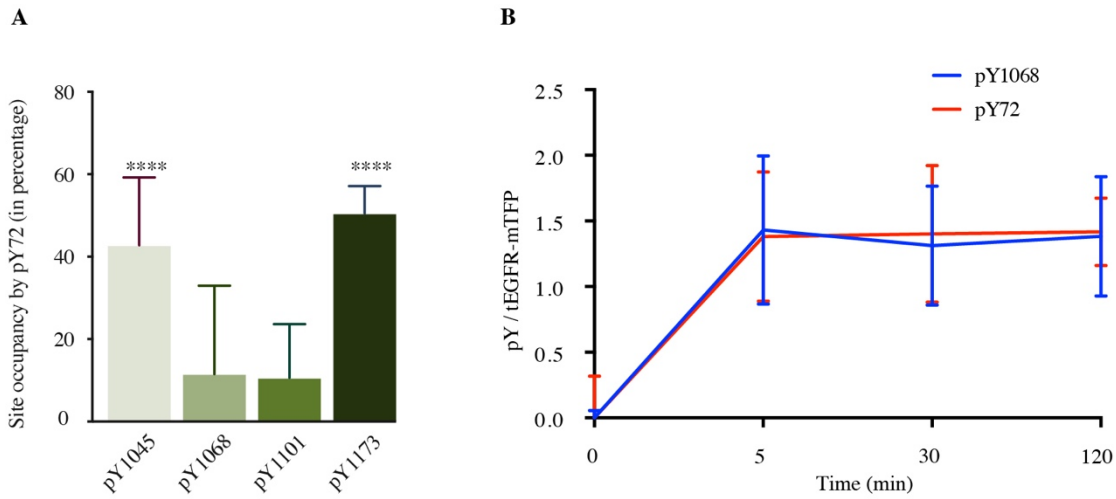

Figure 3- 2 A) Competition based epitope mapping of generic anti-phosphotyrosine pY72. (± SD, n=100-120 cells, **** p<0.0001). B) Temporal phosphorylation EGFR profile obtained upon ectopic EGFR-mTFP expression and 5P-200ng EGFR stimulation using pY72 and anti-EGFR pY1068 antibody on western blots

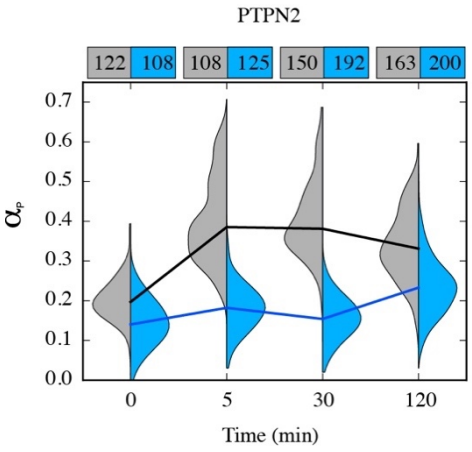

Figure 3- 3 Exemplary temporal EGFR-mTFP phosphorylation profiles (grey, control; blue; co-PTPN2-mCitrine expression) The violin plots show the α distributions from single cells stimulated with 200ng/ml 5P-EGF (number of cells denoted on top of the plots, medians at different time points are connected).

reactivity of an enzyme is not always a reflection of its interaction with its substrate. To determine regulation of the temporal response of pEGFR to 5P-EGF stimulation by PTPs, high-content imaging experiments were performed. MCF7 cells ectopically expressing EGFR-mTFP and PTP_x-mCitrine were stimulated for 0, 5, 30 and 120 min with 200ng 5P-EGF and were chemically fixed. EGFR has 6-7 signaling tyrosine residues and the phosphorylation dynamics of these individual residues are not clear. Therefore, we used a generic anti-phosphotyrosine antibody (PY72) (Grecco et al., 2010)to identify most of the phosphorylated tyrosine residue on EGFR. Epitope mapping experiments showed that PY72 predominantly binds to pY1045 and pY1173 sites of EGFR (Figure 3-2). As this antibody can potentially identify phosphorylated tyrosine on every protein in a cell, a FRET-FLIM approach was used to calculate the fraction of EGFR that interacts with PY72-CY3.5. The fluorescent protein mTFP at the C-terminal of EGFR acts as a FRET donor to Cy3.5 dye conjugated to PY72. To confirm that the temporal profile obtained by PY72 reflects EGFR signaling, lysates of MCF7 cells ectopically expressing EGFR-mTFP and stimulated with 5P-200ng were blotted and stained with PY72 and an anti-pY1068 antibody which represents a Grb2 mediated signaling tyrosine residue. The sustained EGFR phosphorylation temporal profile for both PY72 and pY1068 demonstrated that PY72 follows the EGFR signaling response. Using a in-house built automated microscopy set-up we were able to acquire 50 fields of views with 7-12 cells per field. This provided us with enough cells to exploit the cell to cell variance in PTP expression and determine enzymatic strength of each PTP over time on EGFR phosphorylation.

The temporal EGFR phosphorylation profile represented as PFC_α (wheren in, $PFC_\alpha = \alpha_{control} / \alpha_{PTPx}$) with ectopic PTP_x-mCitrine expression shows that ER-localized PTPN2 and predominantly plasma membrane localized PTPRE/RF/RG/RJ strongly dephosphorylate ligand activated EGFR as compared to the other PTPs (Figure 3-3).

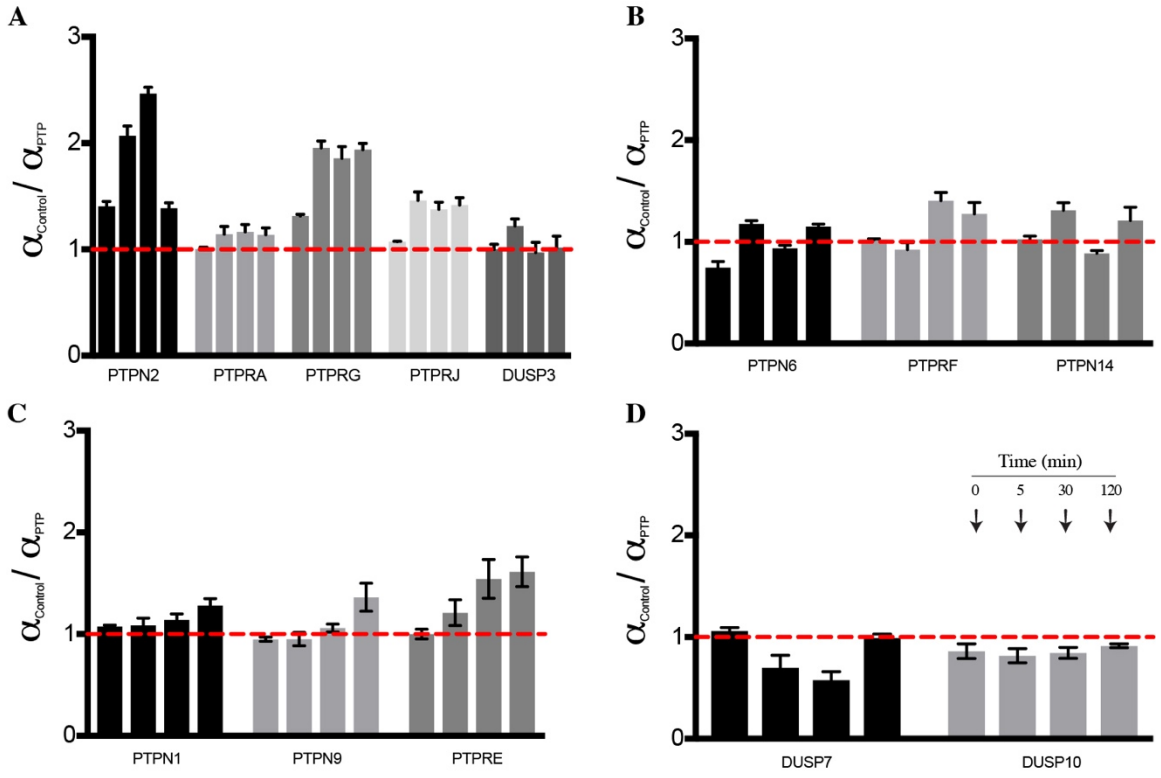

Figure 3- 4 Interleaved temporal bar plots of median EGFR phosphorylation fold-changes($\alpha_{ctr}/\alpha_{PTP}$ ±MAD n~150 cells per condition) upon ectopic PTP_X-mCitrine expression stimulated 5P-200ng EGFR for 30 min and 120 min time-point.

Although these PFC_α profiles provided a general view of a cellular population in regulating phosphorylation-dephosphorylation of EGFR in presence of a particular PTP, it does not account for the variance in PTPx-mCitrine expression in each cell that can affect EGFR differently (Figure 3-4). Generally, to our observation Receptor-PTPs are expressed weakly as compared to the cytosolic or ER-bound PTPs. A catalytically weak phosphatase will be required in high concentration as compared to a potent phosphatase in dephosphorylating EGFR with similar magnitude.

As we obtained nearly 50-100 cells for each PTP_X per stimulation time-point, it was possible to determine an impact of varied PTP_X –mCitrine expression on pEGFR by correlating the alpha to PTPx-mCitrine expression in each cell. The p values obtained by spearman

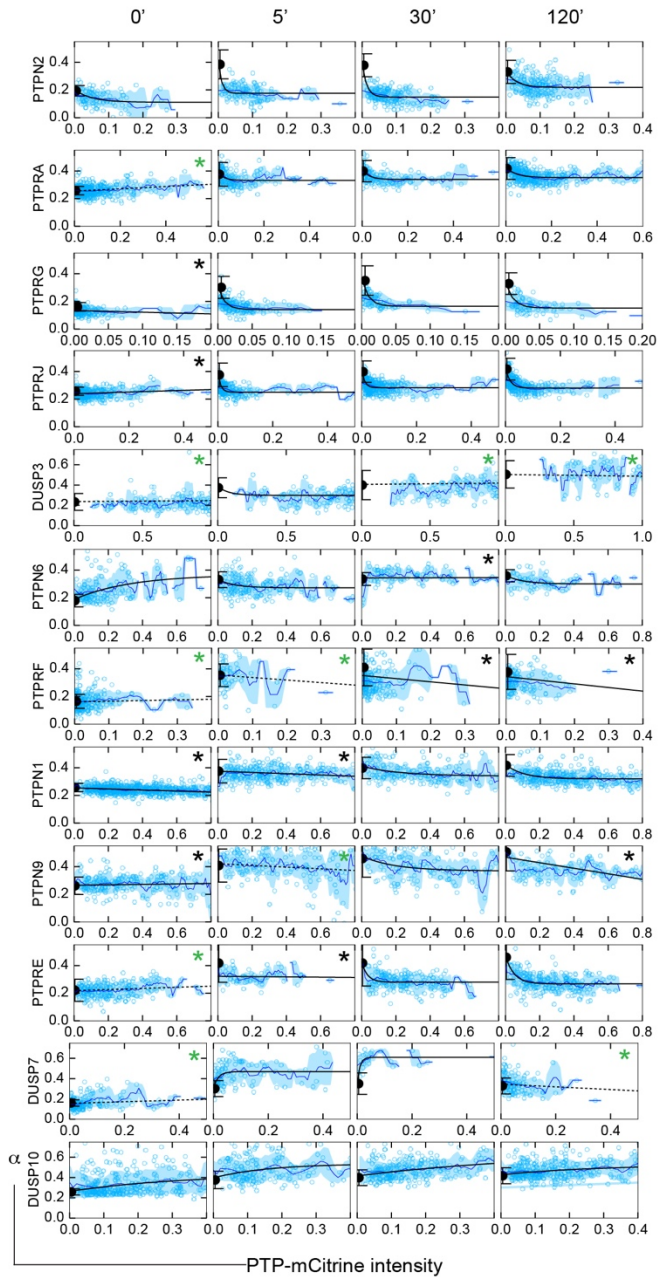

Figure 3- 5 α vs. PTP_X-mCitrine single cell fluorescence scatter plots. Black circle: mean α_{ctr}±SD; black lines: exponential fits (* - linear fit for weak dependence, green asterisk: distributions of α_{ctr} and α_{PTP} did not significantly differ); blue lines with error bounds: moving averages with standard deviations.

correlation ranking (Figure 3-5) showed that at all time point for PTPRF, there is no correlation between alpha and PTPx-mCitrine expression. Implying there might be another parameter that can play a role in regulating PTPRF effect on EGFR.

To determine the strength of each PTPs, median alpha of the control was anchored on to the Y-axis from which an exponential/linear fit to the scatter plot was drawn. The slopes (linear fit) or initial slopes (exponential fit) of α vs. PTP_X-mCitrine fluorescence intensity were calculated for each EGF stimulation time point (Figure 3-5). This showed that the ER

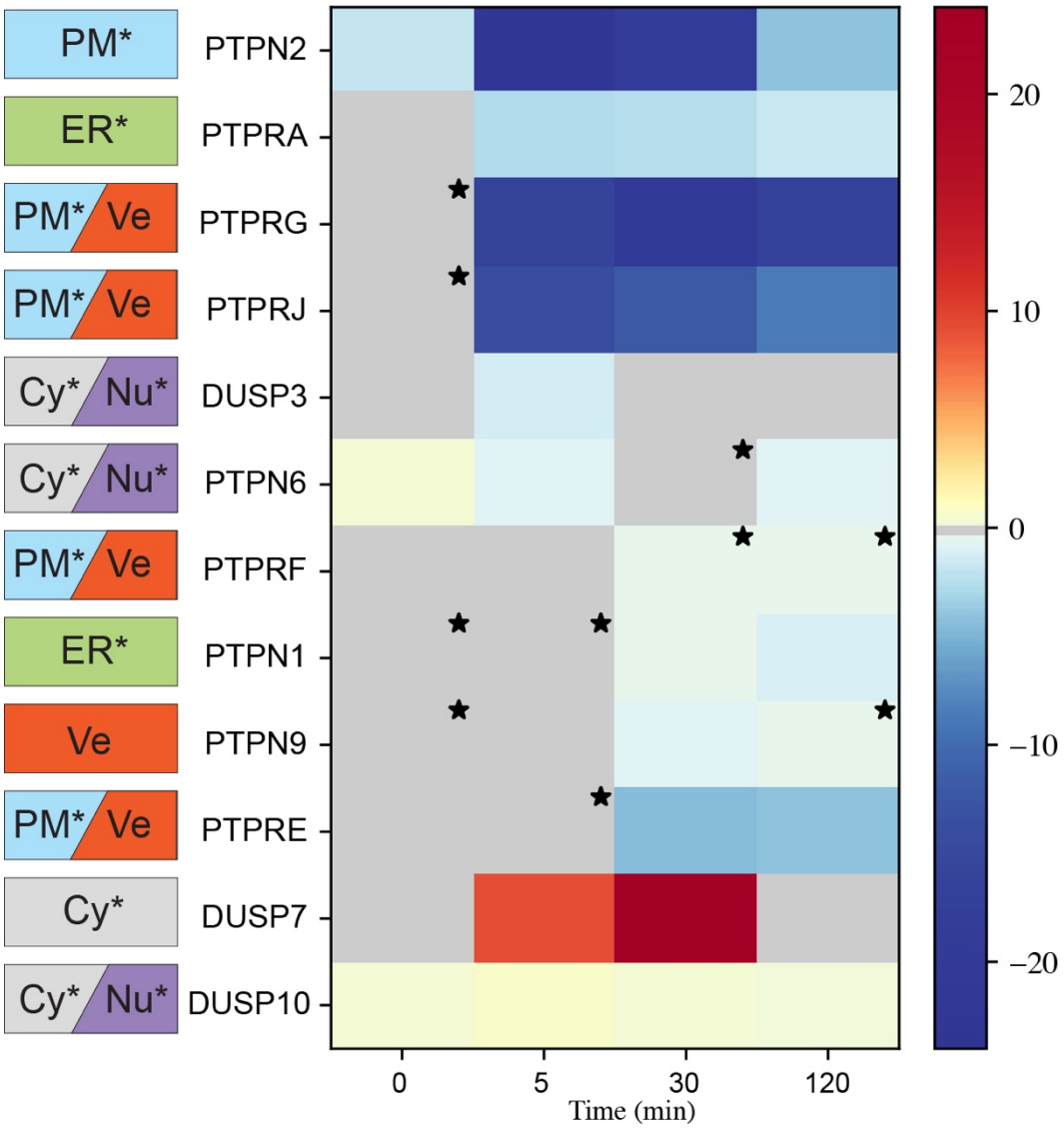

Figure 3- 7 Relative specific PTPX-mCitrine activities for 0, 5, 30 and 120min after 200ng/ml 5P-EGF of stimulation with respective subcellular localization of PTPX-mCitrine.

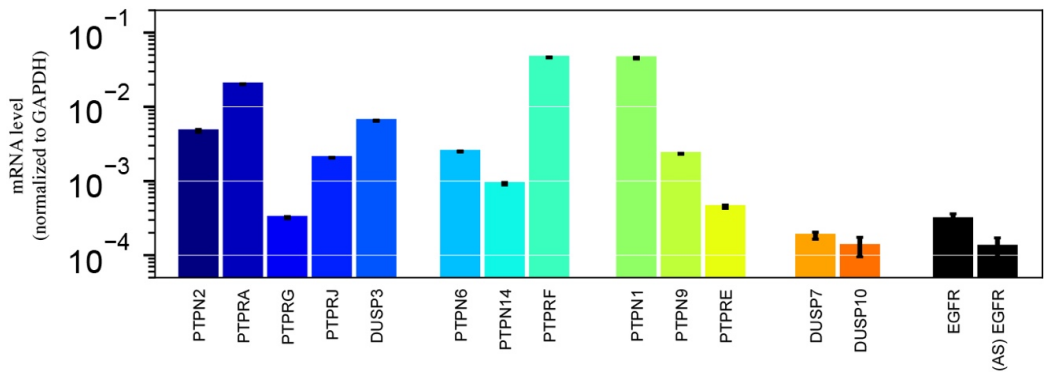

Figure 3- 6 PTP_X and EGFR mRNA levels in MCF7 cells obtained from micro arrays (relative to GAPDH mRNA). AS: anti-sense.

localized PTPN2 and the PM localized PTPRG/RJ are the strongest regulators of EGFR phosphorylation. PTPRA and DUSP3, on the other hand, turned out to act weakly on the phosphorylated EGFR. As opposed to PFC_{α} , the PTPx specific activity revealed PTPRE to be a weak phosphatase compared to that of PTPRJ (Figure 3-6). The mRNA expression profiling of MCF7 cells showed that PTPRG is expressed weakly in these cells as compared to the cytosolic/ER-PTPs (Figure 3-7). This, in conjunction with the effect seen upon siRNA silencing, corroborates its high activity. Interestingly, the mRNA profiling results also showed that MCF7 cells have a very low expression of EGFR, validating our approach of ectopic expression of EGFR to understand the role of PTPs on EGFR phosphorylation.

The strong phosphatase activity of PTPN2 prior to EGF stimulation, implies its role in regulating autonomously activated EGFR hence validating its role in the safeguard mechanism. The strong regulation of pEGFR upon stimulation by juxtaposed subcellular localized ER-PTPN2 and PM-RG/RJ indicates they might play a specific role in regulating cell response upon ligand stimulation. As PY72 detects certain tyrosine residues of EGFR more efficiently, other phosphatases might play a role in regulating specific EGFR tyrosine sites, for e.g. pY845 which is important for autocatalysis (Baumdick et al., 2015; Sato, 2013).

3.3 VESICULAR COMPONENTS PLAY AN IMPORTANT ROLE IN EGFR TRAFFICKING

Vesicular trafficking is an essential machinery that brings RTK to phosphatase activity rich perinuclear region (Baumdick et al., 2015; Sabet et al., 2015). Upon binding to its ligand at the plasma membrane, EGFR gets internalized through a clathrin dependent/independent mechanism (Mayor et al., 2017) (See:Section 1.3). Ligand mediated EGFR activation leads to phosphorylation of Y1045 that acts as a binding site to cCbl, a ubiquitin ligase which adds ubiquitin to the lysine residues at the EGFR kinase domain(Grovdal et al., 2004). To

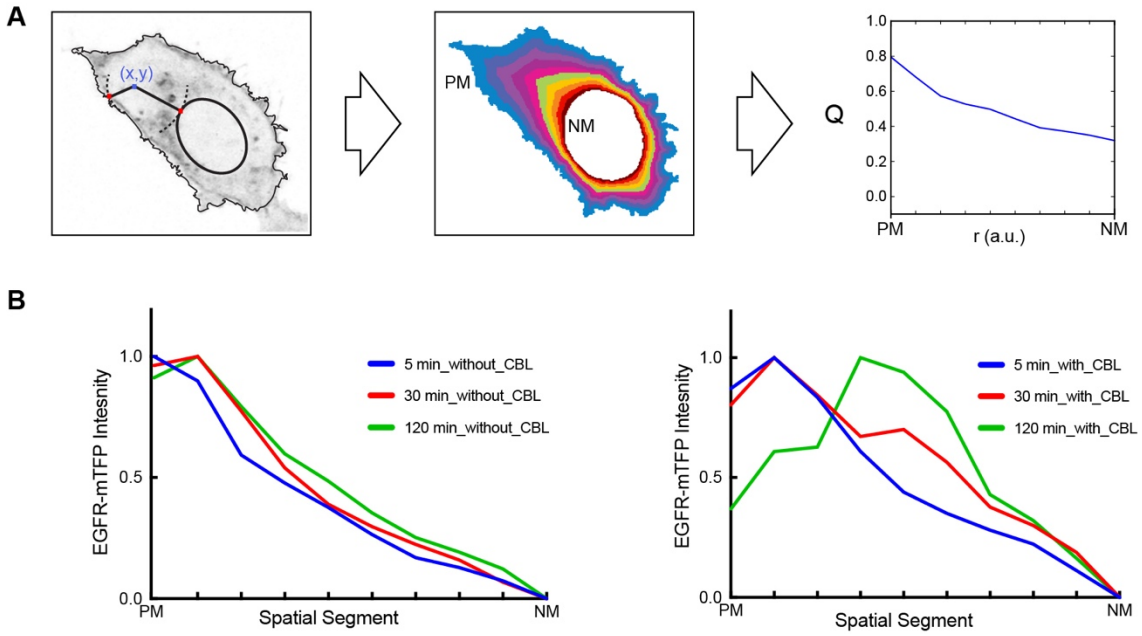

Figure 3- 8 A) Dimensionality reduction from Cartesian (x, y) to normalized radial (r) distribution of quantity (Q) between the plasma (PM) and the nuclear (NM) membrane. B) Averaged radial profile of EGFR-mTFP fluorescence obtained from MCF7 cells ectopically expressing EGFR-mTFP along with or without co-ectopic expression of cCbl-BFP. Cells were stimulated with 200ng/ml 5P-EGF and chemically fixed. n=~30 cells

determine how cCbl influences 5P-EGF stimulated EGFR internalization, MCF7 cells ectopically expressing both EGFR-mTFP and cCbl-BFP or only EGFR-mTFP were stimulated with 200ng of 5P-EGF. The distribution of EGFR in the cell was determined by obtaining a radial profile for each individual cell Each cell was masked by using the EGFR-mTFP intensity images and the nuclei were obtained from cCBL-BFP intensity images by using CellProfiler. For each pixel within the cell, the distance to the closest plasma membrane (PM) and nuclear membrane (NM) were calculated to derive a normalized distance $r = r_{PM} / (r_{PM} + r_{NM})$ (Figure 3-8). All pixels were split in 10 intervals according to their normalized distances. The mean value was calculated for each segment for each observable, yielding a radial profile for the individual cells (Figure 3-8).

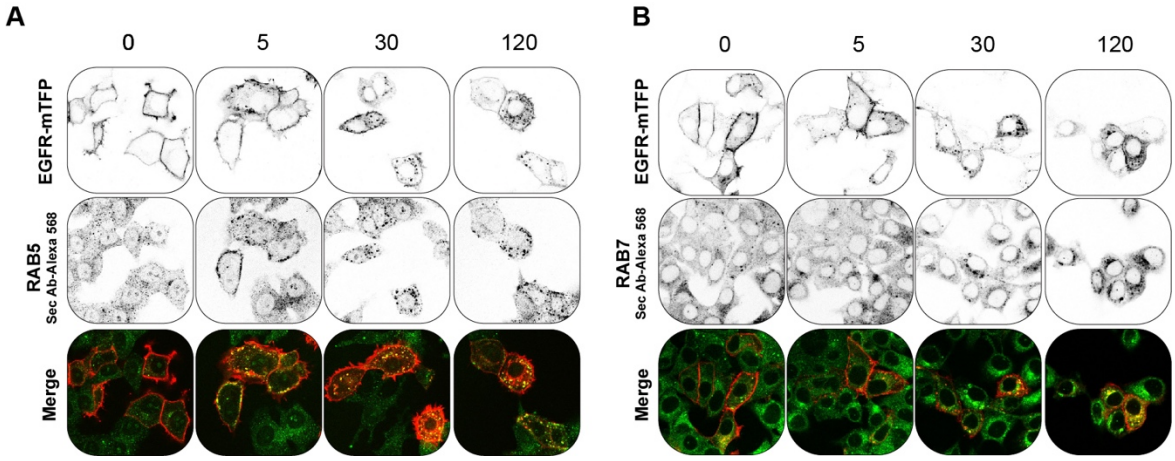

Figure 3- 9 A) Exemplary merged (third row) and individual image sets of EGFR-mTFP and anti-RAB5-Alexa568 fluorescence for 0,5,30 and 120min after 200ng/ml 5P-EGF stimulated and chemically fixed MCF7 cells. B) Similar set of images are represented for RAB7.

The averaged radial profile for ~30 cells showed that EGFR is internalized and is distributed to the perinuclear region with time in presence of cCbl-BFP (Figure 3-8). The internalization however occurs through small vesicles that fuse to RAB5 positive early endosomes (Bucci et al., 1992). These early endosomes then mature into Rab7 positive late endosomes through which EGFR is directed to lysosomes for degradation (Vanlandingham and Ceresa, 2009). The immunostaining for RAB5 and RAB7 shows that upon EGF stimulation, EGFR colocalizes with RAB5 positive endosomes near the plasma membrane and is distributed in the cell. At late time points, EGFR colocalizes with the perinuclear RAB7 positive compartment suggesting molecules that are subjected to degradation. A small fraction of EGFR in the RAB5 positive early endosomes at 120min (Figure 3-9) shows a consistent activity of the vesicular trafficking machinery in distributing activated EGFR. The signaling EGFR molecules that escape this unidirectional trafficking, i.e. not subjected to lysosomal degradation are deactivated by a complimentary mechanism, that is, via dephosphorylation by PTPs.

3.4 How PTPs modulate EGFR recycling?

A complete shutdown of EGFR signaling requires its trafficking to perinuclear area where it interacts with ER-PTPs. Considering phosphorylation of EGFR Y1045 site serves as a docking site for cCbl that ubiquitinates EGFR availing an efficient internalization, regulation of this site by PTPs affect its trafficking to lysosomes; instead they allow recycling of EGFR back to the plasma membrane (Baumdick et al., 2015; Grovdal et al., 2004; Ravid et al., 2004). To examine how strong negative regulator PTPN2, PTPRG and PTPRJ affect pEGFR Y1045, MCF7 cells ectopically expressing EGFR-mTFP, cCbl-BFP and PTPx-Citrine were stimulated with 5P-200 ng EGF and were chemically fixed before staining it with EGFR-pY1045 following immunostaining protocol.

As represented in Figure 3-10, in the control condition i.e. cells expressing EGFR-mTFP and cCbl-BFP, massive phosphorylation of EGFR at the plasma membrane at early time-point indicates ligand stimulation is necessary for an efficient phosphorylation of pY1045. Interestingly, at 120 min most of the EGFR molecules were dephosphorylated in the

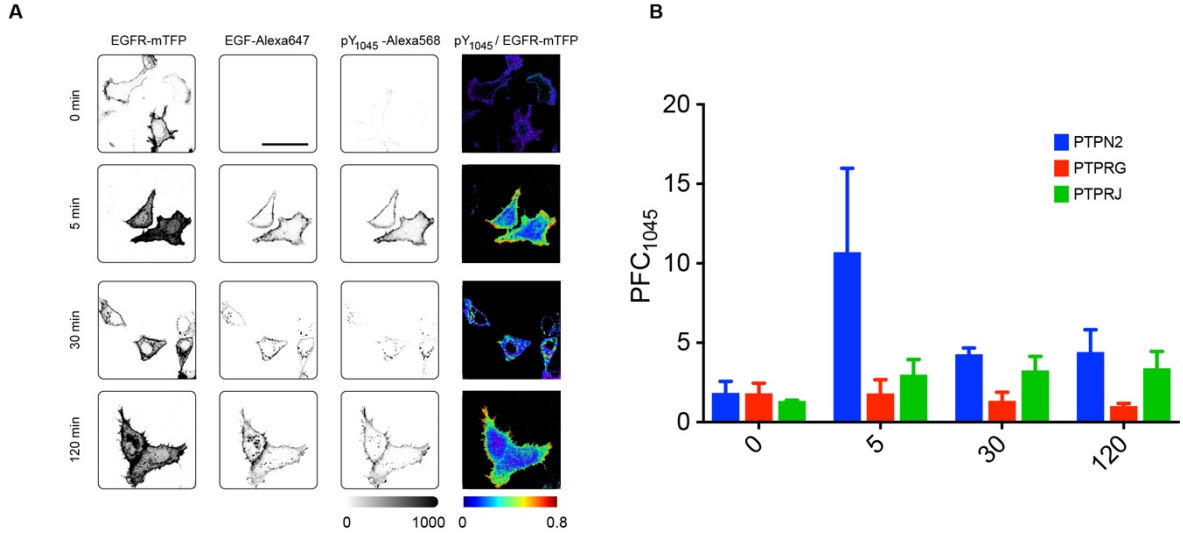

Figure 3- 10 A) Exemplary image sets of EGFR-mTFP, EGF-Alexa647, anti-pY_{1045}-Alexa568 fluorescence and phosphorylated pY_{1045} fraction (pY_{1045}/EGFR-mTFP) at 0,5,30 and 120min after 200ng/ml 5P-EGF stimulation of MCF7 cells Scale bar: 50µm. B) Phosphorylation fold change PFC_{1045} upon ectopic expression of PTPN2, PTPRG or PTPRJ; n~30-40 cells

perinuclear region, which entails that the endogenous ER-PTPs like PTPN1 and PTPN2 are capable of acting efficiently on ectopically expressed EGFR-mTFP. However, the phosphorylated fraction of EGFR molecules at the plasma membrane at late time points implies autocatalytic activity of the monomeric EGFR molecules that are recycled back to the plasma membrane and that act on other ligandless EGFR molecules. To evaluate how phosphorylation of EGFR Y1045 is affected upon PTP_X expression, PFC_{pY1045} ($cDNA - PFC_{pY1045/PTPx} = \frac{(pY1045/EGFR)_{ctr}}{(pY1045/EGFR)_{PTPx}}$) for each time point was determined. This showed that PTPN2, PTPRG and PTPRJ significantly affected phosphorylation of pY1045. Among the three PTPs, PTPN2 and PTPRG had a stronger effect on pY1045 phosphorylation before stimulation indicating its role in inhibiting internalization or promoting recycling of spontaneously activated EGFR molecules. The increase in activity over EGFR by PTPN2 and PTPRJ show their role in acting on liganded receptors. PTPRG on the other hand showed a sustained activity indicating it has no or very less impact of ligand bound EGFR molecules.

3.5 Spatial distribution of PTPRG, PTPN2 and PTPRJ determines its interaction with EGFR

To assess how PTP_X distribution is affected upon EGF stimulation, calculated radial profiles for each timepoint (Figure 3-8) and reconstructed 3D spatial-temporal maps (STM) to represent distribution of EGFR-mTFP, liganded EGFR (EGF-Alexa647/EGFR-mTFP) and PTPx-mCitrine in space and time. We also generated STMs for the α_{TM} for PTPN2 and PTPRG/J to understand how the PTP distribution correlates with their interaction with EGFR.

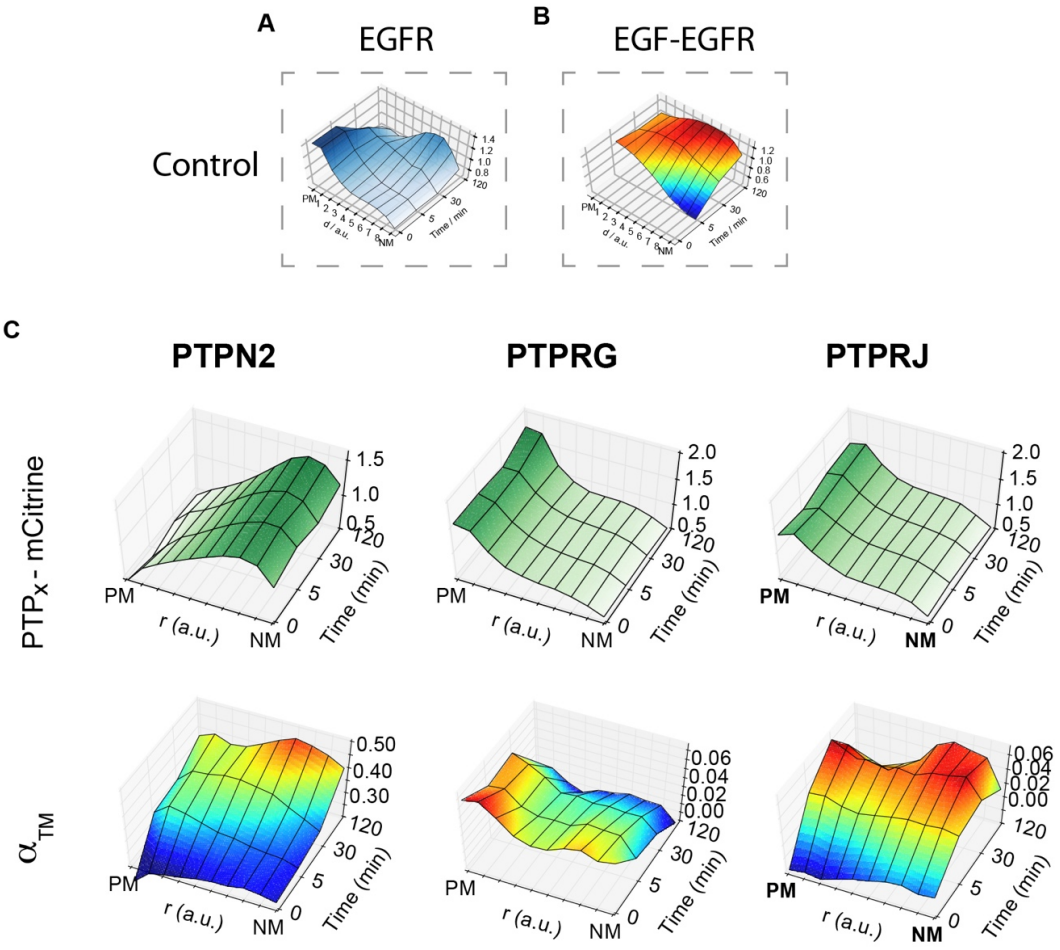

Figure 3- 11 STMs depicting A) EGFR-mTFP fluorescence and B) calculated fraction of EGFR bound to EGD (EGF-EGFR) C) PTP_X-mCitrine fluroscence (top) and fraction of EGFR-mTFP interacting with PTP_X^{TM}-mCitrine (bottom) (TM-PTPN2 (C216S); PTPRG (C1060S); PTPRJ (D1205A))

The STM of EGFR-mTFP shows that the EGFR present on the plasma membrane is distributed to the perinuclear region at late time point which constitutes mostly EGFR molecules that are bound to EGF (STM of EGF-EGFR). The PTPx-STMs showed that PTPN2-mCitrine is predominantly localized in the perinuclear area but is also present in lower amount near the cell. This explains its ability to interact with EGFR at early-time points (Figure 3-11) and to strongly dephosphorylate pY1045 (Figure 3-10) and hence plays a major role in maintaining ligandless EGFR on the plasma membrane. The increased interaction with EGFR at later time-points hints that PTPN2 acts on liganded receptors and can regulate the temporal phosphorylation profile. PTPRG/RJ-mCitrine, on the other hand showed higher concentrations at the plasma membrane, which further increased upon EGF stimulation. The increase in translocation upon EGF stimulation suggests PTPRG/RJ employs the EGFR vesicular trafficking machinery. Unlike PTPRJ that showed an increase in interaction with liganded EGFR, PTPRG-mCitrine interacted with monomeric EGFR (unstimulated) and did not show any increase in interaction upon stimulation. This indicates that PTPRG directly interacts with the recycling ligandless EGFR and hence possibly plays an important role in determining EGFR-EGF response properties. By interacting with liganded EGFR, PTPRJ regulates the temporal profile of EGFR phosphorylation similar to PTPN2 but due to its presence on the plasma membrane, at later time points it is able to dephosphorylate any spontaneously activated EGFR.

3.5 Spatial temporal maps for $EGFR_{pY1068}$ reveals local PTP activity

pY1068 is a Grb2 binding site through which the EGFR signal is propagated to the downstream proteins. To learn how spatially distributed PTPs coupled with differential vesicular dynamic system regulate EGFR signaling, we observed changes in phosphorylation of Y_{1068} in space and time.

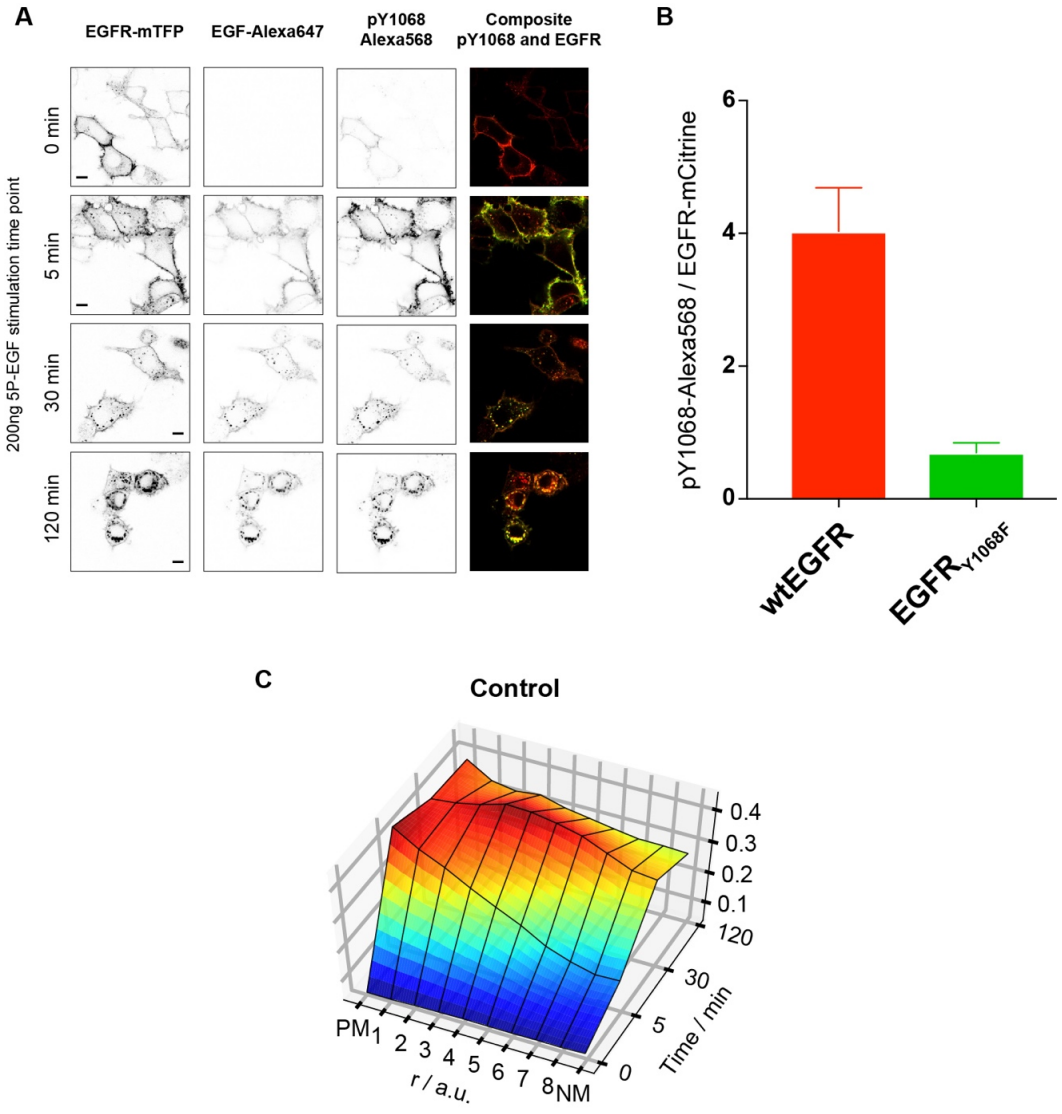

Figure 3- 12 Exemplary image sets of EGFR-mTFP, EGF-Alexa647, anti-pY_{1068}-Alexa568 fluorescence and phosphorylated pY_{1068} fraction (pY_{1068}/EGFR-mTFP) at 0,5,30 and 120min after 200ng/ml 5P-EGF stimulation of MCF7 cells Scale bar: 50µm. B) Immunofluorescence based antibody specificity test C) STMs depicting phosphorylation response on pY_{1068} signaling site (n~90, N=4).

The specificity of pY1068 was determined by immunofluorescence experiment using MCF7 cell expressing wild type EGFR-mCitrine or EGFR-Y1068F-mCitrine. The reduced staining in case of EGFR-Y1068F-mCitrine proves that the antibody is specific to pY1068 site of EGFR (Figure 3-12 B). Spatial EGFR phosphorylation profile i.e. $STM_{pY1068\text{-}norm}$ (ratiometric immuno-pY_{1068}-Alexa 568/EGFR-mTFP fluorescence) shows that the pY1068 phosphorylation increased at the plasma membrane upon stimulation (Figure 3-12 A and C), while at 30 mins the signal mainly came from the internalized liganded EGFR molecules present in endosomes. To generate these STM maps only cells falling in the lower 15-35% of mTFP intensity range were chosen to avoid any artifact caused due to the ectopic expression of EGFR-mTFP. Therefore, an increase in phosphorylation of EGFR molecules at the plasma membrane can be accredited to the autocatalytic activity of the recycled ligandless EGFR.

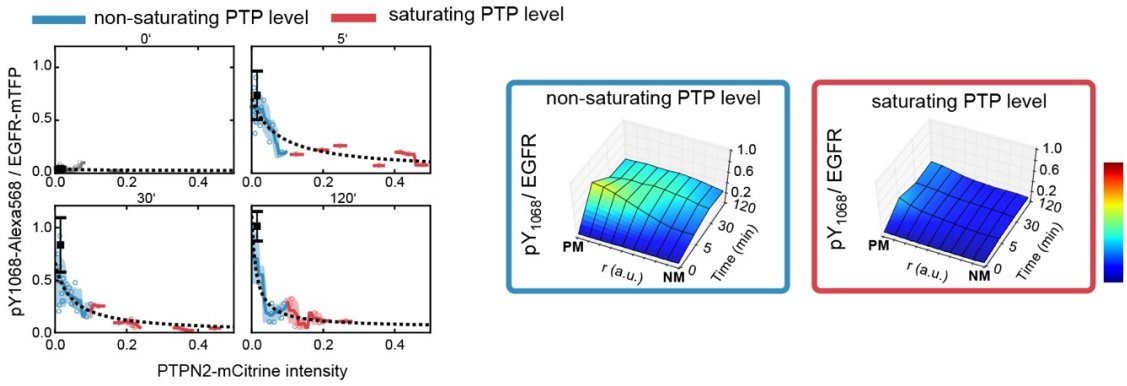

Figure 3- 13 Left: pY_{1068}/EGFR vs. PTPN2-mCitrine fluorescence scatter plots were used to determine the PTPN2-mCitrine fluorescence intensity threshold at which saturation of EGFR dephosphorylation occurs. Blue/red circles: single cells with low/high PTPN2-mCitrine intensity with respect to saturation threshold (below/above); solid lines and shaded bounds: corresponding moving averages and standard deviation.

To determine the local specific activity of the ER-PTPN2 and receptor PTPRG/RJ over EGFR Y1068 phosphorylation, we derived the ratiometric maps of phosphorylation fold-change ($cDNA - PFC_{pY1068/PTPx} = \frac{(pY1068/EGFR)_{ctr}}{(pY1068/EGFR)_{PTPx}}$) upon ectopic PTP_X-mCitrine expression and ($siRNA - PFC_{pY1068/PTPx} = \frac{(pY1068/EGFR)_{ctr}}{(pY1068/EGFR)_{PTPx}}$) upon siRNA mediated PTP_x silencing. In order to also avoid overexpression artifacts on EGFR dephosphorylation, we analyzed cells with PTP_X-mCitrine expression levels where EGFR phosphorylation was sensitive to the perturbation and disregarded cells with high or saturated concentration of PTPx as exhibited by the mCitrine intensity (Figure 3-13). Receptor-PTPs are weakly expressed as compared to the ER or cytosolic PTPs. Therefore, the $cDNA - PFC_{pY1068/PTPN2}$ were scaled by the corresponding average of the PTPx-mCitrine intensity. This scaling factor allowed us to compare the activity of differently expressed PTPs over EGFR.

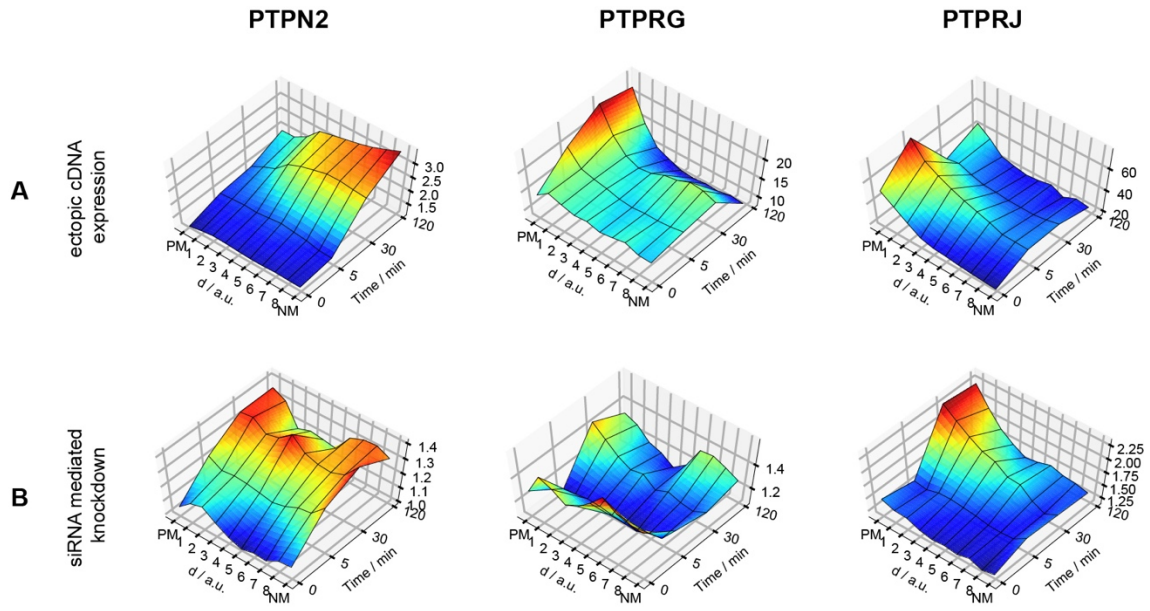

Figure 3- 14 STMs showing effect of A) PTP_X-mCitrine expression (top-row) on phosphorylation fold-change (PFC-cDNA) reflecting the relative PTP_X-mCitrine reactivity towards pY_{1068} upon 5P-EGF (n~60, N=3). B) Corresponding PFC-siRNA is shown in the second row (n~30, N=3).

Both $cDNA - PFC_{pY1068/PTPx}$ and $siRNA - PFC_{pY1068/PTPx}$ (Figure 3-14) showed that PTPN2 dephosphorylated ligand activated EGFR. The dephosphorylation was confined mainly to the perinuclear region in case of ectopic expression of PTPN2-mCitrine upon 5P-EGF stimulation. siRNA mediated knockdown of PTPN2 showed an effect on EGFR phosphorylation extended to the periphery of a cell. This reciprocal perturbation experiment proves that the ER-PTP like PTPN2 is crucial in determining signal duration. Not only it had an effect on liganded EGFR, but by acting on unstimulated EGFR it showed that PTPN2 plays an important role in shutting down the autocatalytic activity of an autonomously activated ligandless EGFR molecule.

Although local phosphatase activity of PTPRG/RJ is limited to the plasma membrane (Figure 3-14), their ability to act differently on liganded and ligandless EGFR associate them to a specific role in regulating EGFR response. PTPRG strongly dephosphorylated EGFR before stimulation. However, its activity was affected upon GF stimulation at early timepoint implying an underlying biochemical regulation like GF triggered ROS mediated inhibition of its activity. At later time points, an increase in dephosphorylation of EGFR at the plasma membrane further emphasizes the role of PTRPG in regulating ligandless EGFR. PTPRJ, unlike PTPRG, is possibly immune to the EGF triggered ROS mediated inhibition and hence showed a considerable effect on EGFR phosphorylation at 5 min. Like PTPN2, PTPRJ has a role in suppressing prolonged signaling from liganded receptors.

3.6 PTPRG STRONGLY AFFECT ENDOSOMAL SIGNALING

Upon interacting with pY1068 of EGFR, Grb2 interacts with other protein complexes and turns on a specific downstream signaling like e.g. MAPK or AKT (Gan et al., 2010). Rapid changes in terms of the architecture of the plasma membrane due to assembly of the proteins occurs upon GF stimuli. Vesicular trafficking not only shuttles liganded and ligandless

receptors to different phosphatase regions or to lysosomal degradation, but it also provides a compartment for a sustained downstream signaling. To determine how PTPx affect phosphorylation of Y1068 on the endosomal EGFR, we identified endosomes by using EGF-Alexa 647 intensity images and extracted different measurable values for the identified endosomes like intensity of Alexa 568 (pY1068) and mTFP (EGFR) for each time point (Figure 3-15 A). The number of endosomes was normalized to the total number of cells for each time point. This analysis showed that upon 5P-EGF stimulation at 30 min for the control, there is a wide distribution of EGFR Y1068 phosphorylated endosomes that has two peaks. Considering, the cells were stimulated with 5P-EGF, at 30min the variation in endosomal EGFR phosphorylation is mainly due to mixture of low to high number of phosphorylated receptors per endosomes (Villaseñor et al., 2015, 2016). At 120 min, however, lower phosphorylation of EGFR per endosomes shows the effect of endogenous perinuclear PTPs (Figure 3-15 B).

Upon ectopic expression of PTPN2, PTPRG or PTPRJ, EGFR phosphorylation on endosomes was highly compromised both at 30 and at 120 min (Figure 3-15 C). PTPN2 and PTPRJ both allow weak endosomal signaling that is evident from the skewness in distribution towards the left side of the plot. PTPRG, on the other hand, is capable of shutting complete endosomal signaling mainly due to its own activity coupled with highly expressed endogenous ER-PTPs. Although this proves that PTPs play an important role in regulating endosomal downstream signaling, the difference in PTPRG and PTPN2/PTPRJ suggest that they might also regulate specific downstream signaling.

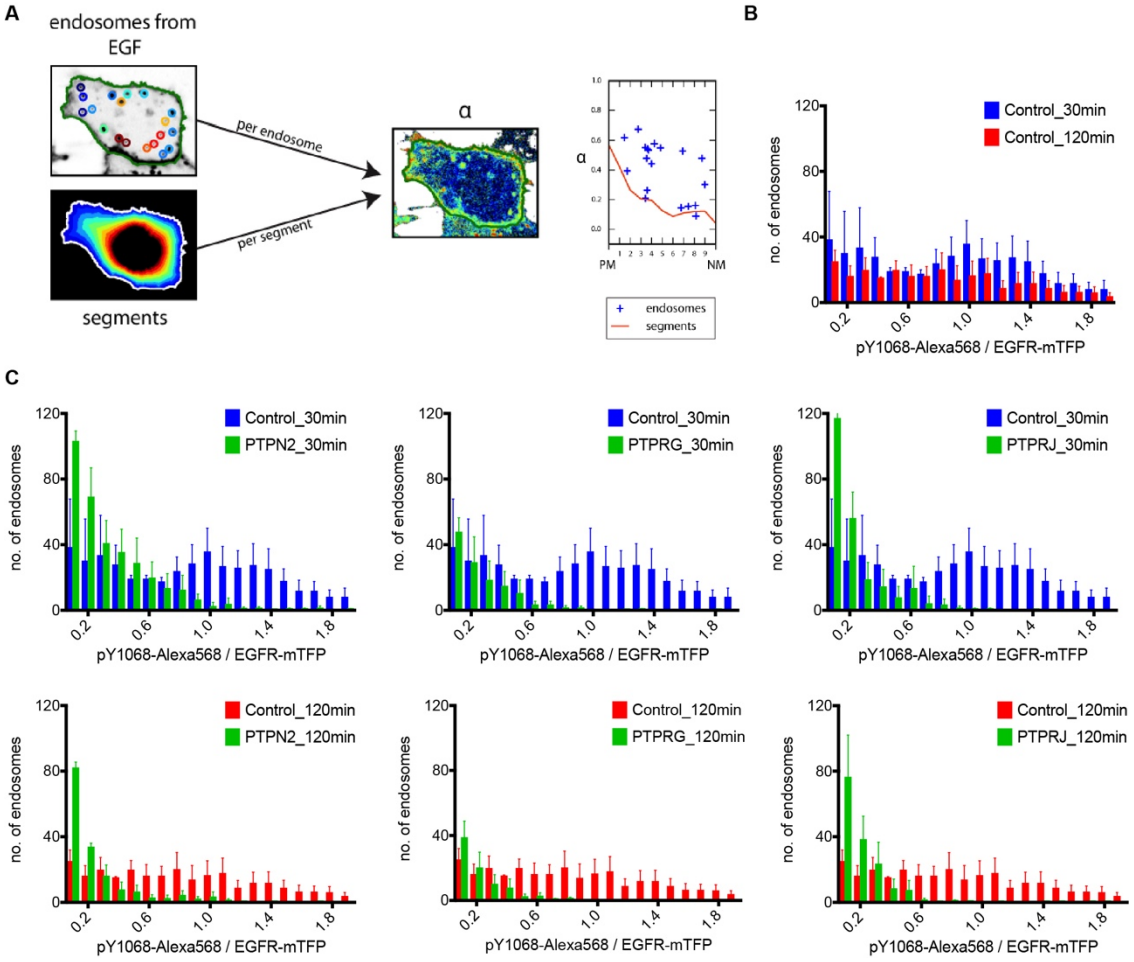

Figure 3- 15 A) Identification of endosomes for each timepoint by using EGF-Alexa647 images in a python based-Segmentor tool. Distribution of the fraction of EGFR phosphorylated at pY1068 per endosomes for B) control at 30 min and 120 min (n~90, N=4) and C) upon ectopic expression of PTP_X-mCitrine (n~60, N=3) (top row=30min; bottom row=120 min)

DISCUSSION

Ligand binding elevates the intrinsic kinase activity of EGFR, leading to phosphorylation of its C terminal tyrosine residues and allows binding of adaptor proteins that transduces signal to the downstream protein (Arkhipov et al., 2013; Kovacs et al., 2015; Schlessinger, 2002; Shan et al., 2012; Wagner, Stacey, Liu, & Pawson, 2013). Ligand bound EGFR at the plasma membrane is ubiquitinated and is internalized in vesicles that integrates with early endosomes maturing to late endosomes (LEs) which eventually fuse with lysosomes where the receptors are denatured and degraded (Bucci et al., 1992; Levkowitz et al., 1999; Rink, Ghigo, Kalaidzidis, & Zerial, 2005; Villaseñor, Kalaidzidis, & Zerial, 2016). ER-PTPs like PTPN1 have been reported as regulators of liganded EGFR (Baumdick et al., 2015) but they also act on monomeric ligandless EGFR and thus facilitate EGFR to recycle back to the plasma membrane via Rab11-recycling endosomes.(Baumdick et al., 2015; Ullrich, Reinsch, Urbé, Zerial, & Parton, 1996). This report implies that the vesicular dynamics is an integral part in regulating EGFR activity.

From literature, it is known that PTPRG expression is downregulated in breast cancer (Panagopoulos et al., 1996), nasopharyngeal carcinoma (Kwok et al., 2015) and chronic myeloid leukemia (Della Peruta et al., 2010). The gene expression is repressed mainly due to hypermethylation of CpG island in its promoter region (Della Peruta et al., 2010; Xiao et al., 2014). PTPRJ is frequently deleted in breast, colon and thyroid cancers (Iuliano et al., 2004; Ruivenkamp et al., 2002). There is a study that shows PTPRJ expression is higher in the invasive breast cancer cells like MDA-MB-231, Hs578T and BT-549 as compared to the less invasive cells like MCF7, T47D, SKBR3 and MCF10A (Spring et al., 2015). ER-PTP like PTPN2 gene expression is low in the breast cancer cells (Shields et al., 2013). This gene

is lost in triple negative breast cancer (Shields et al., 2013). Upon reconstituting PTPN2 levels in these cell lines, it was observed that cell proliferation was impaired. Although SHP2 is the only PTP that has been identified as an oncogene (Loh et al., 2003; Tartaglia et al., 2001) there are few PTPs like PTPN1, PTPRA and PTPRF whose physiological role is unclear. (Nanney, Davidson, Gates, Kano, & King, 1997; Tanner et al., 1996; Yang et al., 2005; Yip, Saha, & Chernoff, 2010) (Gu et al., 2017; Tabiti, Smith, Goh, & Pallen, 1995). (LeVea, McGary, Symons, & Mooney, 2000). As most of these cell lines show an elevated RTK activity and have dysfunctionality in phosphatase indicates that inhibition of PTPs is one an important mechanism to maintain RTK signalling. Although few large-scale screening and many individual studies have investigated the role of PTPs in RTK signaling (Barr et al., 2009; Liu & Chernoff, 1997; Tarcic et al., 2009; Tiganis, Bennett, Ravichandran, & Tonks, 1998; Yao et al., 2017; Yuan, Wang, Zhao, & Gu, 2010), they all lack the temporal and spatial resolution to know 'when' and 'where' the spatially segregated PTPs acts on a RTK like EGFR. By using a quantitative imaging of EGFR phosphorylation, EGFR-PTP interactions studies and decomposing phosphorylation:dephosphurlation cycle in space, we identified endoplasmic reticulum (ER) associated PTPN2 and plasma membrane associated receptor-like PTPRG/J as strong, direct negative regulators of EGFR that along with vesicular machinery of a cell determine RTK functionality.

4.1 ER-LOCALIZED PTPN2 AND PM LOCALIZED PTPRG/RJ ARE STRONG REGULATOR OF EGFR

To compare the strength at which the identified PTPs act on EGFR, we measured how EGFR-mTFP phosphorylation profiles were affected by ectopic PTP_X-mCitrine expression (Figure 3.6). The specific activity of each PTPs were calculated from scatter plots of the fraction of phosphorylated EGFR (α) against PTP_X-mCitrine fluorescence intensity in each cell at each time point (Figure 3.5). This analysis showed that PTPN2 and PTPRG/RJ are

strong regulator of EGFR (Figure 3.6). As discussed earlier, the strong activity of ER-PTPs like PTPN2 is mainly due to their structure that higher affinity towards RTKs like EGFR that possesses phosphorylated tyrosine residues embedded in acidic/basic/ neutral sequences (Barr et al., 2009; Sarmiento et al., 2000; Selner et al., 2014). Dr Stefan Knapp lab in University of Oxford showed that PTPRG and PTPRJ (Barr et al., 2009) act strongly on the peptide that mimics the amino acid sequence of the C-terminal tail of EGFR with a pY1068 residue. Considering the strong effect on EGFR phosphorylation was exhibited by spatially segregated PTPs like ER-bound PTPN2 and plasma membrane bound PTPRG/J, vesicular trafficking becomes an important machinery by which EGFR shuttles between plasma membrane and ER. These experiments were carried out with MCF7 cells ectopically expressing EGFR-mTFP and PTP_X-mCitrine in absence of cCBL-BFP. Ectopic expression of cCBL is necessary for an efficient internalization of ectopically expressed EGFR-mTFP (Figure 3.8)(Ravid, Heidinger, Gee, Khan, & Goldkorn, 2004). This might explain why PTPN1, a known regulator of EGFR (Baumdick et al., 2015; Liu & Chernoff, 1997) showed a weak dephosphorylation activity towards EGFR at late time point. This information also suggests that dephosphorylation of EGFR by PTPN2 is due its fraction that extends to the periphery of a cell (Figure 3.6, Figure 3.11).

4.2 PTPRG HAS AN AFFINITY TOWARDS LIGANDLESS EGFR

By using a cell array fluorescence lifetime imaging microscopy (CA-FLIM) (Grecco et al., 2010) and a reciprocal genetic perturbation approach we identified four classical PTPs: PTPN2/PTPRA/RG/RJ as non-redundant negative regulator of EGFR (Figure 1.7). In literature, few PTPs have been shown to affect EGFR phosphorylation like PTPN2 acts on SHP2 and Grb2 binding sites pY992 and pY1068 respectively (Scharl, Rudenko, & McCole, 2010; Tiganis et al., 1998). PTPRJ /RG acts on both Grb2 binding sites - pY1068 and pY1086 (Kwok et al., 2015; Tarcic et al., 2009). There are also few papers that show that

PTPs like PTPN1 and PTPN2 directly interact with EGFR. These works, however, do not demonstrate the temporal changes in PTP-EGFR interaction pattern upon GF- stimulation. In this thesis, to understand the mechanism by which PTPs act on EGFR, we mutated the catalytic site of their PTP domain (Blanchetot, Chagnon, Dubé, Hallé, & Tremblay, 2005; Flint, Tiganis, Barford, & Tonks, 1997). These mutations stabilize the interactions between PTP^{TM} and its substrate (Flint et al., 1997). As the PTP^{TM} constructs are tagged with mCitrine and EGFR is tagged with mTFP, it allowed us to assess their interaction by using FRET-FLIM (Figure 3.1). This also helped us in identifying weak and transient interactions, which is not possible assess by using biochemical approaches. PTPs like PTPRA/E/FG and PTPN6 have been shown to interact with EGFR for the first time in this thesis (Figure 3.1). The difference in substrate interaction between ER-PTPs and R-PTP is due to their structure. The structural features of ER-PTPs like PTPN1 and PTPN2 show presence of amino acids like Arg47 that confers substrate recognition plasticity while the presence of Gly259 allows high-affinity binding of substrates (Sarmiento et al., 2000). These features of ER-PTPs allow them to interact with their substrate strongly as compared to other cytosolic or receptor like PTPs (Sarmiento et al., 2000). PTPRG has less preference towards liganded EGFR and more towards ligandless EGFR (Figure 3.1, Figure 3.11) which are predominantly in a monomeric state (Baumdick et al., 2015). PTPN2, on the other hand, interacted strongly at all time-points, while PTPRJ and PTPRA showed stronger interaction only at the late time-point implying they regulate either recycled ligandless EGFR or internalized liganded EGFR (Figure 3.1). As ligandless receptors are mainly recycled to the plasma membrane while liganded EGFR are internalized and trafficked to the perinuclear region, it is necessary to spatially decompose the EGFR interaction/phosphorylation in order to understand the regulation of specific EGFR complexes. The STMs for the α_{TM} of PTPRG indeed showed that it interacts with ligandless EGFR-mTFP at the plasma membrane and did not show

considerable change upon stimulation proving that its major role is in regulating EGFR responsiveness towards EGF. In the same line, an increase in interaction of PTPN2 with EGFR in the perinuclear region suggested an important role in regulating EGFR signaling at a later time-point.

4.3 PTPN2 INCREASES RECYCLING OF EGFR TO THE PLASMA MEMBRANE

The localization sequences of PTPs are important in determining their distribution in cell and its accessibility to substrate (Andersen et al., 2001; Tonks, 2006). Both PTPRG and PTPRJ showed a steep gradient in PTPx-mCitrine distribution from the plasma membrane to the perinuclear region while PTPN2 showed a gradual increase in its concentration. Ligand activated EGFR gets internalized and is distributed to the perinuclear localized Rab7 positive late endosome during which it gets dephosphorylated by ER-PTPs (Figure 3.9). This unidirectional trafficking is highly dependent on ubiquitination of EGFR which in turn depends on phosphorylation of pY1045 (Figure 3.10)(Grovdal, Stang, Sorkin, & Madshus, 2004).

By affecting the pY1045 phosphorylation site in absence and presence of EGF, PTPN2 participate in repopulating the plasma membrane with monomeric EGFR that are internalized by autonomous or EGF dependent activation. While by not showing considerable difference upon EGF stimulation, PTPRG shows to reactive specifically towards ligandless EGFR molecules. This observation aligns with the results of the PTPRG trapping mutant (Figure 3.11), emphasizing that PTPRG amongst other PTPs constitutively acts on the ligandless EGFR and maintain the plasma membrane population by affecting its internalization.

4.4 PTPN2 AND PTPRJ DETERMINE DURATION OF EGFR DOWNSTREAM SIGNAL

The $STM_{pY1068\text{-}norm}$ shows a massive phosphorylation of liganded EGFR at the plasma membrane that gets internalized due to vesicular trafficking (Figure 3.12). As we stimulate with a 5min pulse of 200 ng EGF-Alexa647, we obtain a mixture of liganded and ligandless EGFR at later time points. The ligandless monomeric EGFR is dephosphorylated by endogenous ER-PTPs and is recycled back to the plasma membrane where it is reactivated due to autocatalytic activity of other active ligandless EGFR(Baumdick et al., 2015). Whereas liganded, dimeric EGFR unidirectional traffics to late endosomes where it gets inactivated by dephosphorylation before degradation (Figure 3.9 and Figure 3.11)(Baumdick et al., 2015). To learn how PTPs on juxtaposed membranes affect EGFR signaling from ligandless monomeric and liganded dimeric EGFR, we calculated the phosphorylation fold change (PFC) of cells with ectopic PTP_X expression (PFC-cDNA PTP_X) and of cells with siRNA mediated knock-down (PFC-siRNA PTP_X) from $EGFR_{pY1068}$ immunofluorescence experiments (Figure 3.14). These PFC profiles showed that PTPRG and PTPRJ strongly affected signaling from ligandless EGFR at the plasma membrane while PTPN2 acted on liganded internalized EGFR molecules, implying its role in determining signal duration. PTPRG affected overall endosomal phosphorylation (Figure 3.15) which it can achieve only in association with endogenous perinuclear PTPs like PTPN1 and PTPN2. Both PTPRG and PTPN2 acted on signaling from monomeric EGFR before EGF stimulation, proving that these PTPs collaboratively regulate any spurious signal occurred due to autonomous activation of EGFR. Weak activity of PTPRG as compared to PTPRJ at early stimulation time-point suggests an underlying inhibitory biochemical regulation that affect PTPRG and not PTPRJ. Through other experiments performed in the department, we know that EGF-

mediated ROS generation oxidizes the catalytic cysteine in PTPRG which leads into its inactivation at early time point.

In summary, the negative regulation of PTPRJ and PTPN2 to EGFR assist in dampening prolonged signaling from the plasma membrane and the perinuclear region. The reactive oxygen mediated toggle switch between EGFR and PTPRG at the plasma membrane avails resistance to cells from massive EGFR signaling at low dose of EGF present in the media. By recycling ligandless EGFR after PTPN2 mediated dephosphorylation the vesicular trafficking machinery couples a EGFR-PTPN2 negative feedback to a EGFR-PTPRG toggle switch into a spatially organized network. This network architecture allows the cells to sample their environment for growth factors, to responds at specific doses and to allow downstream signaling in order to determine cell fate.

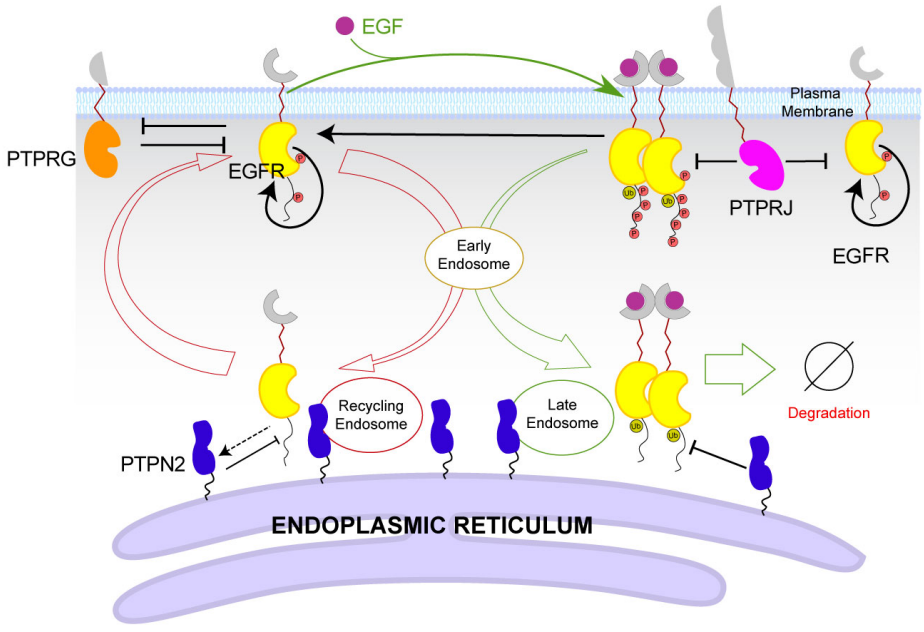

Figure 4. 1 Scheme of the EGFR-PTP interaction network established through EGFR trafficking dynamics. EGFR interacts with PTPRG at the PM and with PTPN2 in the cytoplasm. EGFR trafficking dynamics: ligandless EGFR recycles via early (EE) and recycling endosomes (RE) to the PM (red arrows) whereas upon EGF binding (thin green arrow), ubiquitinated EGF-$EGFR_{Ub}$ unidirectional trafficks via the early- to the late endosomes (LE, green arrow) to be degraded (∅). Causal links are denoted with solid black lines.

REFERENCES

Andersen, J.N., Mortensen, O.H., Peters, G.H., Drake, P.G., Iversen, L.F., Olsen, O.H., Peter, G., Andersen, H.S., Tonks, N.K., Møller, P.H., et al. (2001). Structural and Evolutionary Relationships among Protein Tyrosine Phosphatase Domains. Mol. Cell. Biol. *21*, 7117–7136.

Arkhipov, A., Shan, Y., Das, R., Endres, N.F., Eastwood, M.P., Wemmer, D.E., Kuriyan, J., and Shaw, D.E. (2013). Architecture and membrane interactions of the EGF receptor. Cell *152*, 557–569.

Bánfi, B., Clark, R.A., Steger, K., and Krause, K.H. (2003). Two novel proteins activate superoxide generation by the NADPH oxidase NOX1. J. Biol. Chem. *278*, 3510–3513.

Barr, A.J., Ugochukwu, E., Lee, W.H., King, O.N.F., Filippakopoulos, P., Alfano, I., Savitsky, P., Burgess-Brown, N.A., Müller, S., and Knapp, S. (2009). Large-Scale Structural Analysis of the Classical Human Protein Tyrosine Phosphatome. Cell *136*, 352–363.

Baumdick, M., Brueggemann, Y., Schmick, M., Xouri, G., Sabet, O., Davis, L., Chin, J.W., and Bastiaens, P.I.H. (2015). EGF-dependent re-routing of vesicular recycling switches spontaneous phosphorylation suppression to EGFR signaling. Elife *4*, 1–28.

Belle, L., Ali, N., Lonic, A., Li, X., Paltridge, J.L., Roslan, S., Herrmann, D., W. Conway, J.R., Gehling, F.K., Bert, A.G., et al. (2015). The tyrosine phosphatase PTPN14-Pez inhibits metastasis by altering protein trafficking. Sci. Signal. *8*.

Berrow, N.S., Alderton, D., Sainsbury, S., Nettleship, J., Assenberg, R., Rahman, N., Stuart, D.I., and Owens, R.J. (2007). A versatile ligation-independent cloning method suitable for high-throughput expression screening applications. Nucleic Acids Res. *35*.

Blanchetot, C., Chagnon, M., Dubé, N., Hallé, M., and Tremblay, M.L. (2005). Substrate-trapping techniques in the identification of cellular PTP targets. Methods *35*, 44–53.

Bucci, C., Parton, R.G., Mather, I.H., Stunnenberg, H., Simons, K., Hoflack, B., and Zerial, M. (1992). The small GTPase rab5 function as a regulatory factor in the early endocytic pathway. Cell *70*, 715–728.

Ferguson, K.M. (2008). Structure-based view of epidermal growth factor receptor regulation. Annu. Rev. Biophys. *37*, 353–373.

Fey, D., Matallanas, D., Rauch, J., Rukhlenko, O.S., and Kholodenko, B.N. (2016). The complexities and versatility of the RAS-to-ERK signalling system in normal and cancer cells. Semin. Cell Dev. Biol. *58*, 96–107.

Flint, A.J., Tiganis, T., Barford, D., and Tonks, N.K. (1997). Development of "substrate-trapping" mutants to identify physiological substrates of protein tyrosine phosphatases. Proc. Natl. Acad. Sci. U. S. A. *94*, 1680–1685.

Gan, H.K., Walker, F., Burgess, A.W., Rigopoulos, A., Scott, A.M., and Johns, T.G. (2007). The epidermal growth factor receptor (EGFR) tyrosine kinase inhibitor AG1478 increases the formation of inactive untethered EGFR dimers: Implications for combination therapy with monoclonal antibody 806. J. Biol. Chem. *282*, 2840–2850.

Gan, Y., Shi, C., Inge, L., Hibner, M., Balducci, J., and Huang, Y. (2010). Differential roles of ERK and Akt pathways in regulation of EGFR-mediated signaling and motility in prostate cancer cells. Oncogene *29*, 4947–4958.

Grecco, H.E., Roda-Navarro, P., and Verveer, P.J. (2009). Global analysis of time correlated single photon counting FRET-FLIM data. Opt. Express *17*, 6493–6508.

Grecco, H.E., Roda-Navarro, P., Girod, A., Hou, J., Frahm, T., Truxius, D.C., Pepperkok, R., Squire, A., and Bastiaens, P.I.H. (2010). In situ analysis of tyrosine phosphorylation networks by FLIM on cell arrays. Nat. Methods *7*, 467–472.

Grovdal, L.M., Stang, E., Sorkin, A., and Madshus, I.H. (2004). Direct interaction of Cbl with pTyr 1045 of the EGF receptor (EGFR) is required to sort the EGFR to lysosomes for degradation. Exp. Cell Res. *300*, 388–395.

Gschwind, A., Fischer, O.M., and Ullrich, A. (2004). The discovery of receptor tyrosine kinases: targets for cancer therapy. Nat. Rev. Cancer *4*, 361–370.

Gu, Z., Fang, X., Li, C., Chen, C., Liang, G., Zheng, X., and Fan, Q. (2017). Increased PTPRA expression leads to poor prognosis through c-Src activation and G1 phase progression in squamous cell lung cancer. Int. J. Oncol. 489–497.

Haj, F.G. (2002). Regulation of Receptor Tyrosine Kinase Signaling by Protein Tyrosine

Phosphatase-1B. J. Biol. Chem. *278*, 739–744.

Hunter, T., and Cooper, J.A. (1985). Protein-tyrosine kinases 1. 897–930.

Iuliano, R., Le Pera, I., Cristofaro, C., Baudi, F., Arturi, F., Pallante, P., Martelli, M.L., Trapasso, F., Chiariotti, L., and Fusco, A. (2004). The tyrosine phosphatase PTPRJ/DEP-1 genotype affects thyroid carcinogenesis. Oncogene *23*, 8432–8438.

José, J., Noz, M., Arrega, C., Blanco-Aparicio, C., and Pulido, R. (2003). Differential interaction of the tyrosine phosphatases PTP-SL, STEP and HePTP with the mitogen-activated protein kinases ERK1/2 and p38α is determined by a kinase specificity sequence and influenced by reducing agents. Biochem. J *372*, 193–201.

Jura, N., Shan, Y., Cao, X., Shaw, D.E., and Kuriyan, J. (2009). Structural analysis of the catalytically inactive kinase domain of the human EGF receptor 3. Proc. Natl. Acad. Sci. U. S. A. *106*, 21608–21613.

Kamentsky, L., Jones, T.R., Fraser, A., Bray, M.A., Logan, D.J., Madden, K.L., Ljosa, V., Rueden, C., Eliceiri, K.W., and Carpenter, A.E. (2011). Improved structure, function and compatibility for cellprofiler: Modular high-throughput image analysis software. Bioinformatics *27*, 1179–1180.

Keilhack, H., Tenev, T., Nyakatura, E., Godovac-Zimmermann, J., Nielsen, L., Seedorf, K., and Böhmer, F.D. (1998). Phosphotyrosine 1173 mediates binding of the protein-tyrosine phosphatase SHP-1 to the epidermal growth factor receptor and attenuation of receptor signaling. J. Biol. Chem. *273*, 24839–24846.

Klein, P., Mattoon, D., Lemmon, M.A., and Schlessinger, J. (2004). A structure-based model for ligand binding and dimerization of EGF receptors. Proc. Natl. Acad. Sci. U. S. A. *101*, 929–934.

Kluba, M., Engelborghs, Y., Hofkens, J., and Mizuno, H. (2015). Inhibition of receptor dimerization as a novel negative feedback mechanism of EGFR signaling. PLoS One *10*, 1–21.

Kovacs, E., Das, R., Wang, Q., Collier, T.S., Cantor, A., Huang, Y., Wong, K., Mirza, A., Barros, T., Grob, P., et al. (2015). Analysis of the Role of the C-Terminal Tail in the Regulation of the Epidermal Growth Factor Receptor. Mol. Cell. Biol. *35*, 3083–3102.

Kwok, A., Cheung, L., Chok, J., Ip, Y., Chi, A., Chu, H., Man, M., Leong, L., Mun, J., Ko, Y., et al. (2015). PTPRG suppresses tumor growth and invasion via inhibition of Akt signaling in nasopharyngeal carcinoma. Oncotarget *6*, 13434–13447.

Lemmon, M.A., and Schlessinger, J. (2010). Cell signaling by receptor tyrosine kinases. Cell *141*, 1117–1134.

LeVea, C.M., McGary, C.T., Symons, J.R., and Mooney, R.A. (2000). PTP LAR expression compared to prognostic indices in metastatic and non-metastatic breast cancer. Breast Cancer Res. Treat. *64*, 221–228.

Levkowitz, G., Waterman, H., Ettenberg, S.A., Katz, M., Tsygankov, A.Y., Alroy, I., Lavi, S., Iwai, K., Reiss, Y., Ciechanover, A., et al. (1999). Ubiquitin ligase activity and tyrosine phosphorylation underlie suppression of growth factor signaling by c-Cbl/Sli-1. Mol. Cell *4*, 1029–1040.

Li, M.Z., and Elledge, S.J. (2007). Harnessing homologous recombination in vitro to generate recombinant DNA via SLIC. Nat. Methods *4*, 251–256.

Liu, F., and Chernoff, J. (1997). Protein tyrosine phosphatase 1B interacts with and is tyrosine phosphorylated by the epidermal growth factor receptor. Biochem. J. *327*, 139–145.

Loh, M.L., Vattikuti, S., Schubbert, S., Reynolds, M.G., Carlson, E., Lieuw, K.H., Cheng, J.W., Lee, C.M., Stokoe, D., Bonifas, J.M., et al. (2003). Somatic mutations in PTPN11 implicate the protein tyrosine phosphatase SHP-2 in leukemogenesis. Blood *103*, 2325–2332.

Mayor, S., Parton, R.G., and Donaldson, J.G. (2017). Clathrin-Independent Pathways of Endocytosis.

Millard, S.M., and Wood, S.A. (2006). Riding the DUBway: Regulation of protein trafficking by deubiquitylating enzymes. J. Cell Biol. *173*, 463–468.

Mohrmann, K., Gerez, L., Oorschot, V., Klumperman, J., and Van Der Sluijs, P. (2002). Rab4 Function in Membrane Recycling From Early Endosomes Depends on a Membrane To Cytoplasm Cycle. J. Biol. Chem. *277*, 32029–32035.

Nanney, L.B., Davidson, M.K., Gates, R.E., Kano, M., and King, L.E. (1997). Altered distribution and expression of protein tyrosine phosphatases in normal human skin as

compared to squamous cell carcinomas. J. Cutan. Pathol. *24*, 521–532.

Nishimura, Y., Takiguchi, S., Ito, S., and Itoh, K. (2015). EGF-stimulated AKT activation is mediated by EGFR recycling via an early endocytic pathway in a gefitinib-resistant human lung cancer cell line. Int. J. Oncol. *46*, 1721–1729.

Ogiso, H., Ishitani, R., Nureki, O., Fukai, S., Yamanaka, M., Kim, J.H., Saito, K., Sakamoto, A., Inoue, M., Shirouzu, M., et al. (2002). Crystal structure of the complex of human epidermal growth factor and receptor extracellular domains. Cell *110*, 775–787.

Oliner, J.D., Kinzler, K.W., and Vogelstein, B. (1993). In vivo cloning of PCR products in E. coli. Nucleic Acids Res. *21*, 5192–5197.

Panagopoulos, I., Pandis, N., Thelin, S., Petersson, C., Mertens, F., Borg, ??ke, Kristoffersson, U., Mitelman, F., and ??man, P. (1996). The FHIT and PTPRG genes are deleted in benign proliferative breast disease associated with familial breast cancer and cytogenetic rearrangements of chromosome band 3p14. Cancer Res. *56*, 4871–4875.

Parks, E.E., and Ceresa, B.P. (2014). Cell surface epidermal growth factor receptors increase Src and c-Cbl activity and receptor ubiquitylation. J. Biol. Chem. *289*, 25537–25545.

Della Peruta, M., Martinelli, G., Moratti, E., Pintani, D., Vezzalini, M., Mafficini, A., Grafone, T., Iacobucci, I., Soverini, S., Murineddu, M., et al. (2010). Protein tyrosine phosphatase receptor type ?? is a functional tumor suppressor gene specifically downregulated in chronic myeloid leukemia. Cancer Res. *70*, 8896–8906.

Ravid, T., Heidinger, J.M., Gee, P., Khan, E.M., and Goldkorn, T. (2004). c-Cbl-mediated ubiquitinylation is required for epidermal growth factor receptor exit from the early endosomes. J. Biol. Chem. *279*, 37153–37162.

Regad, T. (2015). Targeting RTK signaling pathways in cancer. Cancers (Basel). *7*, 1758–1784.

Reynolds, A.R., Tischer, C., Verveer, P.J., Rocks, O., and Bastiaens, P.I.H. (2003). EGFR activation coupled to inhibition of tyrosine phosphatases causes lateral signal propagation. Nat. Cell Biol. *5*, 447–453.

Rink, J., Ghigo, E., Kalaidzidis, Y., and Zerial, M. (2005). Rab conversion as a mechanism of progression from early to late endosomes. Cell *122*, 735–749.

Robinson, D.R., Wu, Y.-M., and Lin, S.-F. (2000). The protein tyrosine kinase family of the human genome.

Roda-Navarro, P., and Bastiaens, P.I.H. (2014). Dynamic recruitment of protein tyrosine phosphatase PTPD1 to EGF stimulation sites potentiates EGFR activation. PLoS One *9*.

Ross, S.H., Lindsay, Y., Safrany, S.T., Lorenzo, O., Villa, F., Toth, R., Clague, M.J., Downes, C.P., and Leslie, N.R. (2007). Differential redox regulation within the PTP superfamily. Cell. Signal. *19*, 1521–1530.

Ruivenkamp, C.A.L., van Wezel, T., Zanon, C., Stassen, A.P.M., Vlcek, C., Csikós, T., Klous, A.M., Tripodis, N., Perrakis, A., Boerrigter, L., et al. (2002). Ptprj is a candidate for the mouse colon-cancer susceptibility locus Scc1 and is frequently deleted in human cancers. Nat. Genet. *31*, 295–300.

Sarmiento, M., Puius, Y.A., Vetter, S.W., Keng, Y.-F., Wu, L., Zhao, Y., Lawrence, D.S., Almo, S.C., and Zhang, Z.-Y. (2000). Structural Basis of Plasticity in Protein Tyrosine Phosphatase 1B Substrate Recognition. Biochemistry *39*, 8171–8179.

Sato, K. ichi (2013). Cellular functions regulated by phosphorylation of EGFR on TYR845. Int. J. Mol. Sci. *14*, 10761–10790.

Scharl, M., Rudenko, I., and McCole, D.F. (2010). Loss of protein tyrosine phosphatase N2 potentiates epidermal growth factor suppression of intestinal epithelial chloride secretion. Am. J. Physiol. Gastrointest. Liver Physiol. *299*, G935-45.

Schlessinger, J. (2002). Ligand-induced, receptor-mediated dimerization and activation of EGF receptor. Cell *110*, 669–672.

Ségaliny, A.I., Tellez-Gabriel, M., Heymann, M.F., and Heymann, D. (2015). Receptor tyrosine kinases: Characterisation, mechanism of action and therapeutic interests for bone cancers. J. Bone Oncol. *4*, 1–12.

Selner, N.G., Luechapanichkul, R., Chen, X., Neel, B.G., Zhang, Z.Y., Knapp, S., Bell, C.E., and Pei, D. (2014). Diverse levels of sequence selectivity and catalytic efficiency of protein-tyrosine phosphatases. Biochemistry *53*, 397–412.

Shan, Y., Eastwood, M.P., Zhang, X., Kim, E.T., Arkhipov, A., Dror, R.O., Jumper, J., Kuriyan, J., and Shaw, D.E. (2012). Oncogenic mutations counteract intrinsic disorder in the

EGFR kinase and promote receptor dimerization. Cell *149*, 860–870.

Shields, B.J., Wiede, F., Gurzov, E.N., Wee, K., Hauser, C., Zhu, H.-J., Molloy, T.J., O'Toole, S.A., Daly, R.J., Sutherland, R.L., et al. (2013). TCPTP regulates SFK and STAT3 signaling and is lost in triple-negative breast cancers. Mol. Cell. Biol. *33*, 557–570.

Sonntag, M.H., Ibach, J., Nieto, L., Verveer, P.J., and Brunsveld, L. (2014). Site-specific protection and dual labeling of human epidermal growth factor (hEGF) for targeting, imaging, and cargo delivery. Chem. - A Eur. J. *20*, 6019–6026.

Sorkin, A., McClure, M., Huang, F., and Carter, R. (2000). Interaction of EGF receptor and Grb2 in living cells visualized by fluorescence resonance energy transfer (FRET) microscopy. Curr. Biol. *10*, 1395–1398.

Spring, K., Fournier, P., Lapointe, L., Chabot, C., Roussy, J., Pommey, S., Stagg, J., and Royal, I. (2015). The protein tyrosine phosphatase DEP-1/PTPRJ promotes breast cancer cell invasion and metastasis. Oncogene *34*, 5536–5547.

Sun, J., Lu, S., Ouyang, M., Lin, L.-J., Zhuo, Y., Liu, B., Chien, S., Neel, B.G., and Wang, Y. (2013). Antagonism between binding site affinity and conformational dynamics tunes alternative cis-interactions within Shp2. Nat. Commun. *4*, 2037.

Tabiti, K., Smith, D.R., Goh, H.S., and Pallen, C.J. (1995). Increased mRNA expression of the receptor-like protein tyrosine phosphatase α in late stage colon carcinomas. Cancer Lett. *93*, 239–248.

Tanner, J.J., Parsons, Z.D., Cummings, A.H., Zhou, H., and Gates, K.S. (2011). Redox Regulation of Protein Tyrosine Phosphatases: Structural and Chemical Aspects. Antioxid. Redox Signal. *15*, 77–97.

Tanner, M.M., Tirkkonen, M., Kallioniemi, A., Isola, J., Kuukasjärvi, T., Collins, C., Kowbel, D., Guan, X.Y., Trent, J., Gray, J.W., et al. (1996). Independent amplification and frequent co-amplification of three nonsyntenic regions on the long arm of chromosome 20 in human breast cancer. Cancer Res. *56*, 3441–3445.

Tao, J., Malbon, C.C., and Wang, H.Y. (2001). Insulin Stimulates Tyrosine Phosphorylation and Inactivation of Protein-tyrosine Phosphatase 1B in Vivo. J. Biol. Chem. *276*, 29520–29525.

Tarcic, G., Boguslavsky, S.K., Wakim, J., Kiuchi, T., Liu, A., Reinitz, F., Nathanson, D., Takahashi, T., Mischel, P.S., Ng, T., et al. (2009). An Unbiased Screen Identifies DEP-1 Tumor Suppressor as a Phosphatase Controlling EGFR Endocytosis. Curr. Biol. *19*, 1788–1798.

Tartaglia, M., Mehler, E.L., Goldberg, R., Zampino, G., Brunner, H.G., Kremer, H., van der Burgt, I., Crosby, a H., Ion, A., Jeffery, S., et al. (2001). Mutations in PTPN11, encoding the protein tyrosine phosphatase SHP-2, cause Noonan syndrome. Nat. Genet. *29*, 465–468.

Tenev, T., Keilhack, H., Tomic, S., Stoyanov, B., Stein-Gerlach, M., Lammers, R., Krivtsov, a V, Ullrich, a, and Böhmer, F.D. (1997). Both SH2 domains are involved in interaction of SHP-1 with the epidermal growth factor receptor but cannot confer receptor-directed activity to SHP-1/SHP-2 chimera. J. Biol. Chem. *272*, 5966–5973.

Tiganis, T., Bennett, A.M., Ravichandran, K.S., and Tonks, N.K. (1998). Epidermal Growth Factor Receptor and the Apaptor Protein p52Shc are Specific Substrates of T-Cell Protein Tyrosine Phoshphatase. Mol. Celluar Biol. *18*, 1622–1634.

Tonks, N.K. (2005). Redox redux: Revisiting PTPs and the control of cell signaling. Cell *121*, 667–670.

Tonks, N.K. (2006). Protein tyrosine phosphatases: from genes, to function, to disease. Nat. Rev. Mol. Cell Biol. *7*, 833–846.

Ullrich, O., Reinsch, S., Urbé, S., Zerial, M., and Parton, R.G. (1996). Rab11 regulates recycling through the pericentriolar recycling endosome. J. Cell Biol. *135*, 913–924.

Vanlandingham, P.A., and Ceresa, B.P. (2009). Rab7 regulates late endocytic trafficking downstream of multivesicular body biogenesis and cargo sequestration. J. Biol. Chem. *284*, 12110–12124.

Villaseñor, R., Kalaidzidis, Y., and Zerial, M. (2016). Signal processing by the endosomal system. Curr. Opin. Cell Biol. *39*, 53–60.

Wagner, M.J., Stacey, M.M., Liu, B.A., and Pawson, T. (2013). Molecular mechanisms of SH2- and PTB-Domain-containing proteins in receptor tyrosine kinase signaling. Cold Spring Harb. Perspect. Biol. *5*, 1–20.

Wee, P., and Wang, Z. (2017). Epidermal growth factor receptor cell proliferation signaling

pathways. Cancers (Basel). *9*, 1–45.

Weibrecht, I., Böhmer, S.A., Dagnell, M., Kappert, K., Östman, A., and Böhmer, F.D. (2007). Oxidation sensitivity of the catalytic cysteine of the protein-tyrosine phosphatases SHP-1 and SHP-2. Free Radic. Biol. Med. *43*, 100–110.

Wu, P., Wee, P., Jiang, J., Chen, X., and Wang, Z. (2012). Differential Regulation of Transcription Factors by Location-Specific EGF Receptor Signaling via a Spatio-Temporal Interplay of ERK Activation. PLoS One *7*.

Xiao, J., Lee, S., Xiao, Y., Ma, X., Houseman, E.A., Hsu, L., Roy, R., Wrensch, M., Smith, A.J. De, Chokkalingam, A., et al. (2014). PTPRG inhibition by DNA methylation and cooperation with RAS gene activation in childhood acute lymphoblastic leukemia. Int. J. Cancer *135*, 1101–1109.

Yang, J., Groen, A., Lemeer, S., Jans, A., Slijper, M., Roe, S.M., Den Hertog, J., and Barford, D. (2007). Reversible oxidation of the membrane distal domain of receptor PTPα is mediated by a cyclic sulfenamide. Biochemistry *46*, 709–719.

Yang, S.H., Seo, M.Y., Jeong, H.J., Jeung, H.C., Shin, J., Kim, S.C., Noh, S.H., Chung, H.C., and Rha, S.Y. (2005). Gene copy number change events at chromosome 20 and their association with recurrence in gastric cancer patients. Clin. Cancer Res. *11*, 612–620.

Yao, Z., Darowski, K., St-Denis, N., Wong, V., Offensperger, F., Villedieu, A., Amin, S., Malty, R., Aoki, H., Guo, H., et al. (2017). A Global Analysis of the Receptor Tyrosine Kinase-Protein Phosphatase Interactome. Mol. Cell *65*, 347–360.

Yip, S.C., Saha, S., and Chernoff, J. (2010). PTP1B: A double agent in metabolism and oncogenesis. Trends Biochem. Sci. *35*, 442–449.

Yuan, T., Wang, Y., Zhao, Z.J., and Gu, H. (2010). Protein-tyrosine phosphatase PTPN9 negatively regulates ErbB2 and epidermal growth factor receptor signaling in breast cancer cells. J. Biol. Chem. *285*, 14861–14870.

ACKNOWLEDGEMENT

Thank you. If you have cared enough to read this part of thesis it means that you are aware of your contribution in my journey. I am really grateful for your help and encouragement.

I would really like to thank my parents: Mom and Dad and my Tai. Your unconditional support has always encouraged me. I am very lucky to have you in my life.

My mentor-Prof Philippe Bastiaens; I am really honored to meet a teacher like you in an important point of my career. I am really thankful to you for your support during my PhD.

Aneta and Klaus, thanks for your patience. Sven, Angel, Yannick, Maitreyi, Wayne, Martin, Hernan, Lisaweta, Rabea, Jutta, Manuela and Kirsten: working with you guys was a fun and educating experience.

Astrid, Tanja, Christa and Lucia-thank you for your help.

I would also like to thank Prof Andrea Musacchio for accepting my request to be my second examiner.

Current and past members of Department 2, Desi Janata and many people who I befriended in last couple of years: thank you for creating a friendly environment. You guys rock!!!